Geophys. J. Int. (1996) **125**, 229–248

How to reconcile body-wave and normal-mode reference earth models

J.-P. Montagner[1,2] and B. L. N. Kennett[1]

[1] *Research School of Earth Sciences, Australian National University Canberra* ACT 0200, *Australia*
[2] *Institut de Physique du Globe de Paris, 4 Place Jussieu, 75232 Paris* 05, *France*

Accepted 1995 November 20. Received 1995 October 29; in original form 1995 February 24

SUMMARY

Reference earth models can be retrieved from either body waves or normal-mode eigenperiods. However, there is a large discrepancy between different reference earth models, which arises partly from the type of data set used in their construction and partly from differences in parametrization. Reference models derived from body-wave observations do not give access to density, attenuation factor and radial anisotropy. Conversely, reference models derived from normal modes cannot provide the correct locations for the depth of seismic discontinuities, nor the associated velocity jump. Eigenperiods derived from reference models constructed using body-wave data together with classifical attenuation models differ significantly from the observed eigenperiods.

The body-wave and normal-mode approaches can be reconciled. The V_P and V_S velocities given by body-wave models are considered as constraints, and an inversion is performed for parameters that cannot be extracted from body waves in the context of a radially anisotropic model, i.e. the density ρ, the quality factor Q_μ and the anisotropy parameters ξ, ϕ and η. The influence of anelasticity is very large, although insufficient by itself to reconcile the two types of model. However, by including in the inversion procedure the density and the three anisotropic parameters, body-wave models can be brought into complete agreement with eigenperiod data. A number of reference models derived from body waves were tested and used as starting models: *iasp91*, *sp6*, and two new models *ak303* and *ak135*. A number of robust features can be extracted from the inversions based on these different models. The quality factor Q_μ is found to be much larger in the lower mantle than in previous models (e.g. *prem*). Anisotropy, in the form of transverse isotropy with a vertical symmetry axis, is significant in the whole upper mantle, but very small in the lower mantle except in the lower transition zone (between the 660 km discontinuity and 1000 km depth) and in the D″-layer. Compared with *prem* there is an increase of density in the D″-layer and a decrease in the lower transition zone. The attenuation estimates have been derived using velocity dispersion information, but are in agreement with available direct measurements of normal-mode attenuation. Such attenuation data are still of limited quality, and the present results emphasize the need for improved attenuation measurements.

Key words: body waves, earth models, normal modes, seismology.

1 INTRODUCTION

Over the last ten years, the main thrust in seismology has evolved from inversion for spherically symmetric models to the construction of laterally heterogeneous models, which are often termed tomographic models. It might therefore be considered that we have passed beyond a need for inversion for radial reference earth models. However, tomographic models are usually derived from a reference model by linearized inversion schemes based on the use of first-order perturbation theory. The quality of the reference model will strongly condition the outcome of inversions for 3-D models. A number of new reference earth models have been constructed recently based on either body-wave observations or normal-mode observations. The two classes of model provide different types of constraints on earth structure.

Models derived from the body-wave traveltimes reported in the ISC catalogues have primarily been motivated by the desire to achieve more reliable earthquake locations and traveltime tables. Two recent models have been proposed: *iasp91*

(Kennett & Engdahl 1991) and *sp6* (Morelli & Dziewonski 1993). These two models are similar in general, but differ in some respects because they are based on different philosophies. *Iasp91* was designed to try to provide an optimum determination of earthquake location, whereas *sp6* was aimed at the construction of a global average model. Since most seismic stations are located in continental areas, both models are likely to be biased towards continental models, with some compensation in the corrections applied to model *sp6*. Such models derived from body-wave data can only constrain seismic velocity, and they do not contain any information on the density distribution.

The second class of model is derived from normal-mode eigenfrequencies or a mixture of body-wave and normal-mode information. Because the first models were derived from an extensive normal-mode set (1066A, 1066B; Gilbert & Dziewonski 1975), a number of reference earth models have been constructed using eigenfrequency data. The most prominent is probably the *prem* model of Dziewonski & Anderson (1981), which used both normal-mode and body-wave data and also introduced for the first time radial anisotropy in the upper mantle (i.e. transverse isotropy with a vertical symmetry axis). The inclusion of body-wave information improves the resolution of *P*-wave velocities, particularly in the mantle, because many of the observed normal modes are most sensitive to *S* structure. The *prem* model, however, has a number of limitations. It includes a large contrast across a discontinuity at 220 km; subsequent work has suggested that such a feature is unlikely to be of global extent (see e.g. Revenaugh & Jordan 1991). Some aspects of the normal-mode data are not well explained (Montagner & Anderson 1989a), for example fundamental toroidal modes. The body-wave information employed in the construction of *prem* was drawn from a number of sources, and a variety of baseline and tilt corrections were applied for the different phases. The traveltimes derived from the *prem* model give a good general representation of the major phases, but the fit to the ISC information is not as good as that provided by *sp6*.

Recently, Widmer *et al.* (1993) proposed a new model, *core11*, which includes radial anisotropy through the whole earth and includes an attenuation model derived from inversion for the quality factors of the normal modes. Valette & Lesage (1992)

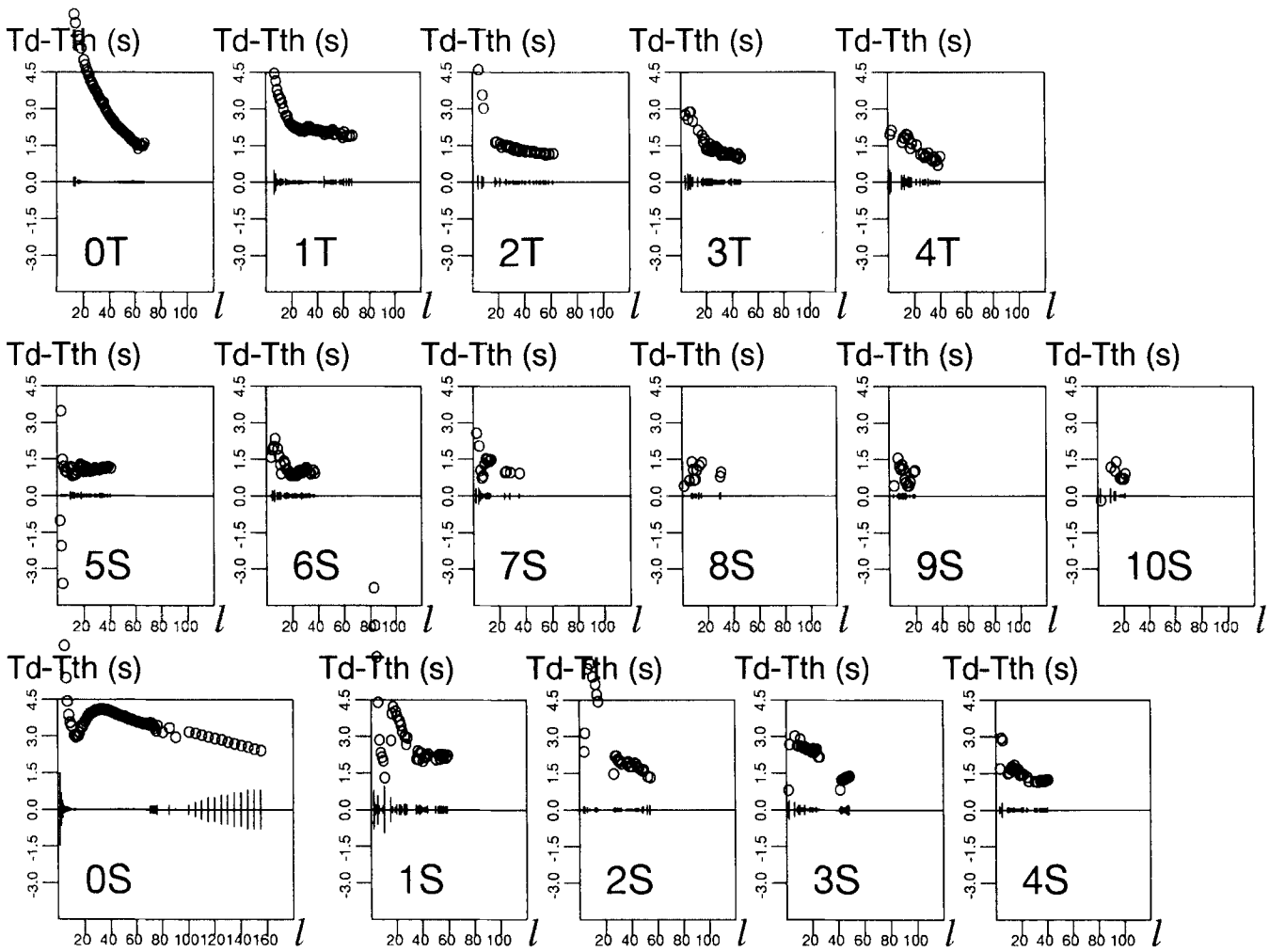

Figure 1. Residuals between eigenperiod data T_d and calculated eigenperiods T_{th} calculated for the model *iasp91* for different branches of spheroidal (S) and toroidal (T) modes according to the angular order l. The radial order n is in the lower corner of each box. The residual $T_d - T_{th}$ is expressed in seconds. The error bar on T_d is plotted on the zero-line. A datum can be considered as explained when T_{th} lies within the error bar.

have shown that it is possible to improve the parametrization of earth models by including pre-stress in the inversion, based on the theoretical development by Valette (1986).

The resurgence of interest in reference earth models in recent years is linked to the need for increased accuracy in the determination of earthquake locations and the delineation of 3-D tomographic anomalies.

2 PHILOSOPHY OF INVERSION—IMPORTANCE OF ANELASTICITY

Most reference earth models were derived for use in some particular applications, and display shortcomings when used for other purposes. For instance, *iasp91* (Kennett & Engdahl 1991) is probably the most suitable model for earthquake location and for calculating traveltimes for the great majority of existing stations, but is biased towards continental structure (and is based on short-period observations). However, when the normal-mode eigenperiods are calculated for this kind of model they are displaced from the observed periods by 1 s or more. Fig. 1 displays the residuals between the eigenperiods calculated from the *iasp91* model and a set of observed eigenperiods, which will be described in more detail in the next section. For each observation, the error bars σ_d are displayed and we can see that there is a large discrepancy between the calculations T_{th} and the observations T_d. To allow a quantitative comparison, we calculate the L_2-measure:

$$\chi = \frac{1}{N_d}\left[\sum_{n=1}^{N_d}\left(\frac{T_{th}-T_d}{\sigma_d}\right)^2\right]^{1/2}, \tag{2.1}$$

which enables us to test whether the data are explained or not.

The body-wave models are constructed for a characteristic period around 1 s, whereas the eigenperiods are derived from measurements at 100 s or longer. So far we have not included the influence of the intrinsic dispersion of wave velocities associated with anelasticity, which is generally invoked to remove the discrepancy between models derived from body-wave and normal-mode observations. We might therefore expect that the large residuals displayed for *iasp91* in Fig. 1 would be reduced by including the influence of attenuation. Fig. 2 shows the same comparison of the calculated and observed eigenperiods as in Fig. 1, but now the *prem* attenuation model has been added to the *iasp91* velocity model and

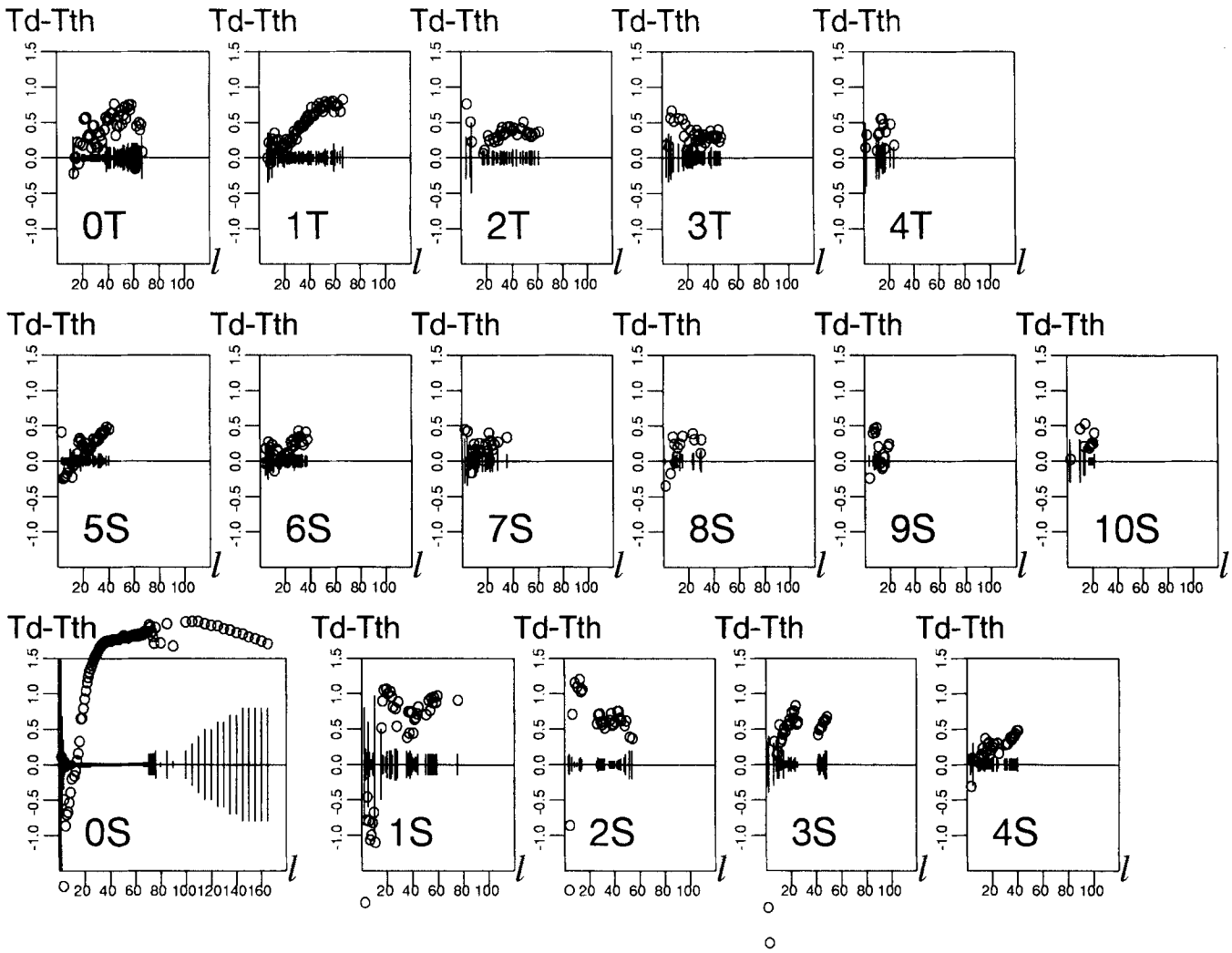

Figure 2. Eigenperiod residual display as in Fig. 1, but now attenuation is taken into account, by incorporating the *prem* model of attenuation with the *iasp91* velocity model in the calculation of eigenperiods.

the *prem* density distribution. There is a decrease in χ from 67.5 to 26.2 but the discrepancy between observed and calculated eigenperiods still prevails. It is important to note that the influence of the attenuation model employed to perform the dispersion corrections is very strong, and even small modifications of the attenuation model can induce large variations in the eigenperiods. The *core11* model of Widmer *et al.* (1993) is a recent reference earth model derived from normal-mode eigenperiods and attenuation. It is not very different from the *prem* model (Dziewonski & Anderson 1981), since it was derived using a linearized inversion with *prem* as the starting model. *Core11*, however, provides a much improved fit compared to *prem* with the attenuation data for normal modes. Even with the *core11* attenuation model coupled to *iasp91*, the discrepancy between observed and theoretical eigenperiods persists.

The model *core11* is based on long-period observations, and, if the seismic velocities are used without attenuation corrections to predict traveltimes, the quality of the traveltime estimates is rather poor. Once the attenuation corrections are made to transfer a 200 s model to 1 s, the fit to the traveltimes is improved. However, neither *prem* nor *core11* provides a satisfactory set of traveltimes for short-period body-wave studies. Kennett, Engdahl & Buland (1996) established a new set of empirical traveltime tables by relocating the entire ISC catalogue using *P* readings with the *iasp91* model. The inferred hypocentral parameters are then used to estimate the traveltimes for a wide variety of phases from the arrival times in the ISC bulletins. About 6000 geographically well-distributed events account for nearly 25 per cent of the ISC readings and have been used as the base set from which smoothed traveltime tables and variance estimates have been extracted for a broad range of mantle and core phases. One measure of the misfit between the observed traveltimes and the predictions of a particular model is provided by the sum of the L_2 norms of misfit for 18 major phase branches (Kennett *et al.* 1996). For *iasp91* this measure is 6.6, and is somewhat better at 5.6 for *sp6*, which has an improved *P*-wave velocity in the core. These misfit levels can be reduced to 4.4 when a multiphase traveltime inversion is undertaken to produce models *ak303* and *ak135*, which we will consider later. By comparison, for the normal-mode models such as *prem* and *core11* the traveltime misfit measures exceeds 15.0 with only a moderate quality of fit for many phases.

We thus see that there is currently a compatibility problem between models derived from body-wave or normal-mode observations, since neither class provides a fully satisfactory explanation of the other type of data set. In this paper we therefore propose a scheme to reconcile the two approaches. Traveltimes are superior to eigenperiods for deriving *P*- and *S*-wavespeed profiles, the location of discontinuities and associated velocity jumps. By comparison, eigenperiod information gives access to the quality factor, density and the anisotropic parameters of an anisotropic earth. The inversion procedure starts with a body-wave velocity model and then additional parameters which cannot be found from body-wave traveltimes are included in the inversion in order to make the model derived from the procedure compatible with the eigenperiod data set.

2.1 Data

The set of normal-mode eigenperiods ${}_nT_l$ (*n*: radial order, *l*: angular order) that we have used has been assembled from a number of sources. The first is the set of eigenperiods used by Dziewonski & Anderson (1981) to derive the *prem* model. This has been supplemented with period data from Roult *et al.* (1990). The most complete data set is described by Widmer (1991) and represents the compilation of measurements from the La Jolla group which have appeared in Gilbert & Dziewonski (1975), Ritzwoller, Masters & Gilbert (1986, 1988) and Smith & Masters (1989).

Comparison of the data sets reveals some eigenperiods for which the discrepancies between different sets exceed the assigned errors. In this case, the datum is either excluded or the error estimate is increased following the procedure described in Montagner & Anderson (1989b). The modes that have been selected are mostly sensitive to mantle structure. This investigation has not been directed towards retrieval of core structure, but the procedure we use can readily be extended into the core.

530 selected eigenperiods constitute our data space **d**. The data are assumed to be independent, so the data covariance matrix $\mathbf{C}_d$ is supposed to be diagonal: $C_{d_{ij}} = \sigma_i \sigma_j \delta_{ij}$. It would have been possible to add to the eigenperiod data the set of available attenuation data measured or compiled by Widmer (1991). We have chosen to make an *a posteriori* comparison between the quality factors for the normal-mode data and those derived from the inversion procedure. There are two reasons for this: first, Widmer (1991) has demonstrated that the resolution of attenuation data is weak; and second, the uncertainty in the measurement of attenuation coefficients is very large and there may be a systematic bias introduced by the broadening of normal-mode peaks due to lateral heterogeneity within the earth.

2.2 Theoretical background

We assume that the earth is spherically symmetric and can be modelled as a radially anisotropic medium, i.e. a transversely isotropic medium with a vertical symmetry axis. Such a medium can be described using six functions of radius *r*; these are the density ρ, the wavespeeds $V_{PH} = [A/\rho]^{1/2}$, $V_{SV} = [L/\rho]^{1/2}$, and the anisotropic parameters $\xi = N/L$, $\phi = C/A$, $\eta = F/(A - 2L)$, where A, C, F, L, N are the five elastic moduli needed to describe the transversely isotropic medium. In the case of isotropy, V_{PH} and V_{SV} are the P and S wavespeeds and the anisotropic parameters ξ, ϕ and η are unity. We also have to take into account the anelasticity of the earth; the available data do not warrant a more complex parametrization than an isotropic representation in terms of the quality factor for the bulk modulus, Q_κ, and for the shear modulus, Q_μ. Such a parametrization has been employed in most of the recent reference earth models derived from eigenfrequency data (Dziewonski & Anderson 1981; Montagner & Anderson 1989b; Widmer 1991). We did not attempt to invert for Q_κ, which is known to be poorly resolved. To a first approximation, Q_κ^{-1} is very close to zero except in the core.

The parameter set $\mathbf{p}(r)$ thus consists of $\rho(r)$, $V_{PH}(r)$, $V_{SV}(r)$, $\xi(r)$, $\phi(r)$, $\eta(r)$ and $Q_\mu(r)$. Using first-order perturbation theory, we can determine the perturbation of the eigenperiod $\delta_n T_l$ induced by small changes in the parameters $\delta\mathbf{p}(r)$ by

$$\delta_n T_l = \sum_{i=1}^{n_p} \int_{r=0}^{a} \left(\frac{\partial_n T_l}{\partial p_i} \right) \delta p_i(r) \frac{dr}{\Delta h}, \qquad (2.2)$$

where a is the radius of the earth and Δh is a normalization factor. The partial derivatives $\partial_n T_i/\partial p_i$ can be computed by variational procedures, and suitable expressions are given by Takeuchi & Saito (1972) and Dziewonski & Anderson (1981).

We introduce anelasticity via a complex part of the P and S wavespeeds:

$$V_P = \alpha = V_{P0}(1 + iQ_\alpha^{-1}), \qquad V_S = \beta = V_{S0}(1 + iQ_\beta^{-1}). \tag{2.3}$$

It should be noted that there is sometimes some confusion between Q_β^{-1} and Q_μ^{-1}. We also have to account for the

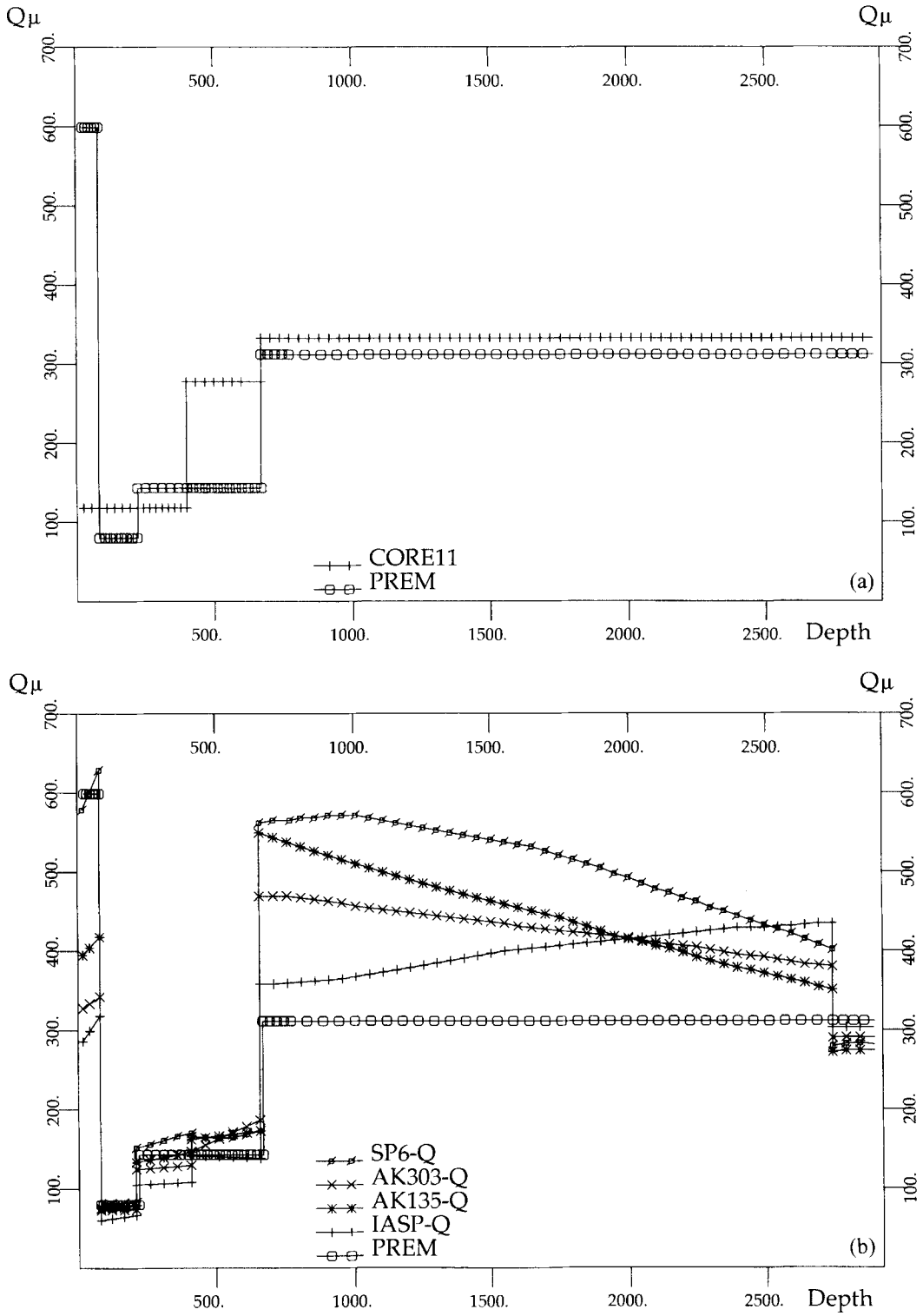

Figure 3. Attenuation models. (a) Starting model: attenuation *prem* model. The *core11* model of Widmer (1991) is shown for comparison. (b) Attenuation models after inversion for Q_μ and ρ only.

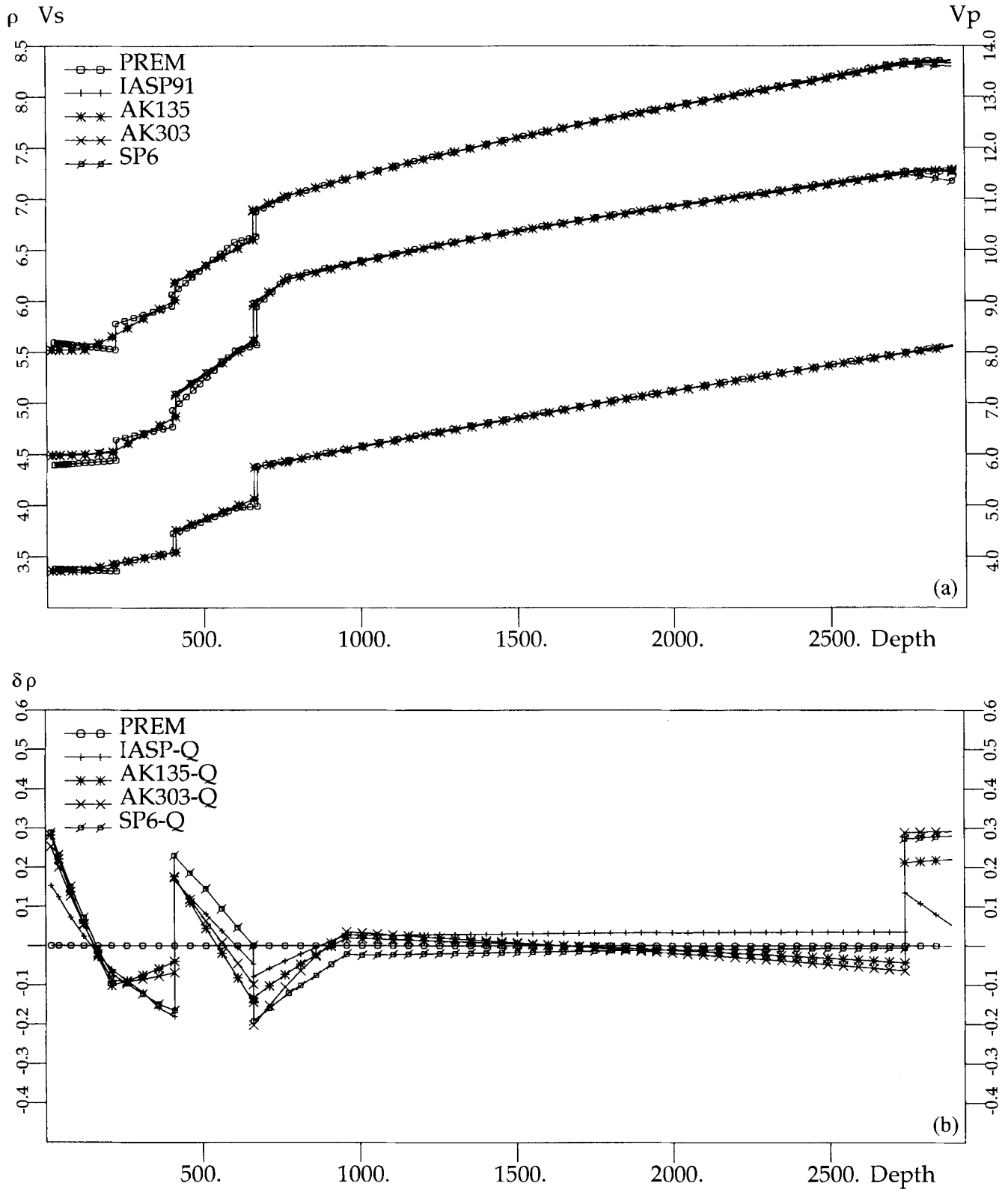

Figure 4. Density models after inversion for Q_μ and ρ only. (a) Starting models for velocities and density. (b) Perturbations in density. (c) Absolute values.

influence of attenuation on the eigenperiods ${}_nT_l$, and have adopted the simple approximation that Q_β is constant over the whole seismic band (1–3000 s). We may then account for the frequency dispersion by using the theory developed by Liu, Anderson & Kanamori (1976) and Kanamori & Anderson (1977) so that

$$C_R(T) = C_R(T_0)\left(1 + \frac{Q_R^{-1}}{\pi} \ln \frac{T_0}{T}\right), \tag{2.4}$$

where $C_R(T)$ is the phase velocity of Rayleigh waves for period

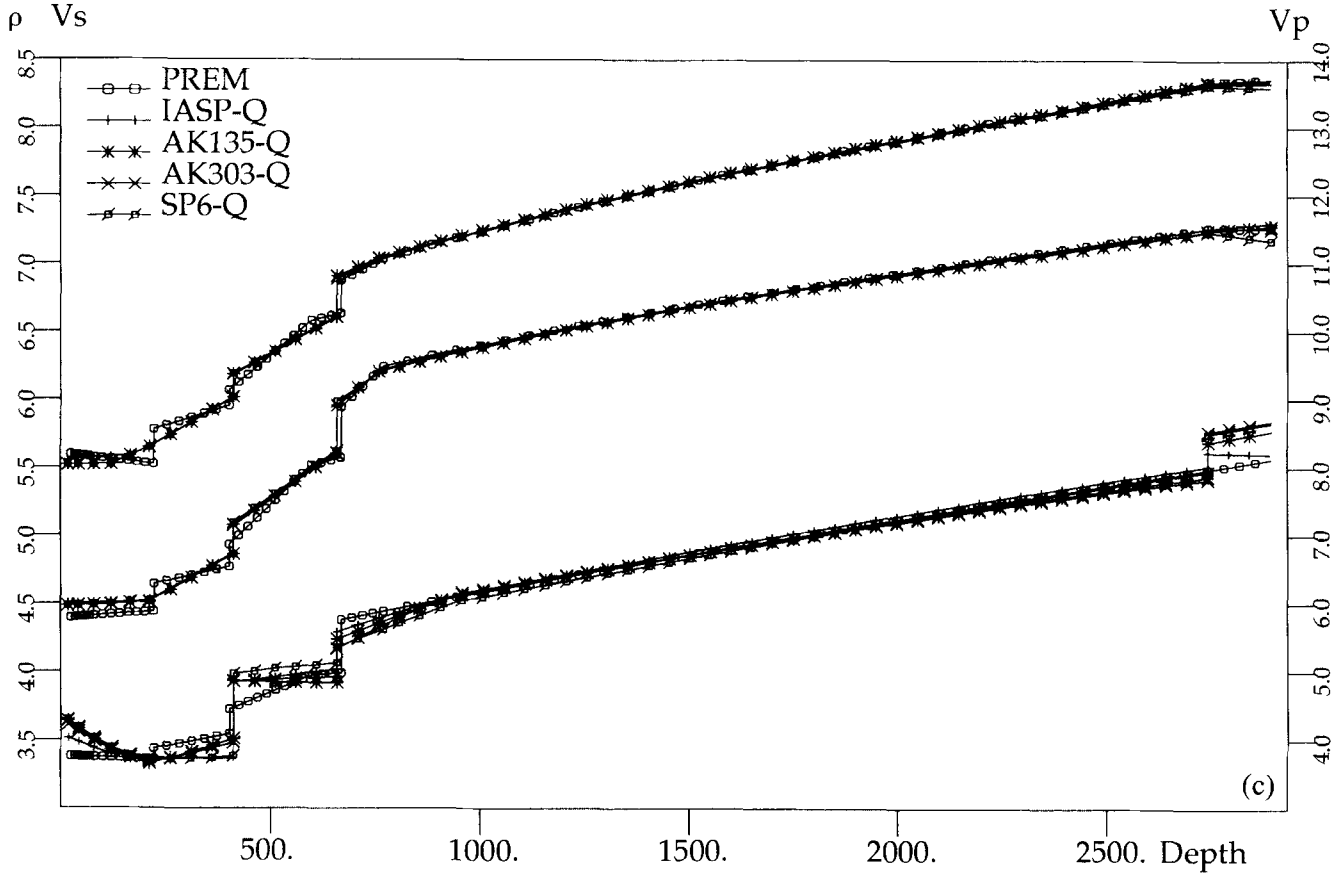

Figure 4. (*Continued.*)

T and T_0 is a reference period which we will take to be 1 s for the body-wave models.

For an isotropic medium the attenuation of $C_R(T)$ is

$$Q_R^{-1}(T) = \int_{r=0}^{r=a} \left(\left(\frac{\beta}{C_R} \frac{\partial C_R}{\partial \beta} \right)_{T,r} Q_\beta^{-1}(r) + \left(\frac{\alpha}{C_R} \frac{\partial C_R}{\partial \alpha} \right)_{T,r} Q_\alpha^{-1}(r) \right) \frac{dr}{\Delta h}, \tag{2.5}$$

where α, β are the P and S wavespeeds. When the attenuation in bulk is negligible throughout the mantle, Q_α^{-1} and Q_β^{-1} are related by

$$Q_\alpha^{-1} = \frac{4}{3}\left(\frac{\beta}{\alpha}\right)^2 Q_\beta^{-1}, \tag{2.6}$$

and from eq. (2.4)

$$\frac{\partial C_R}{\partial Q_R^{-1}} = \frac{C_R(T_0)}{\pi} \ln \frac{T_0}{T}. \tag{2.7}$$

Based on the work of Takeuchi & Saito (1972) and Lee & Solomon (1979), Bussy *et al.* (1993) have showed that the partial derivative of C_R with respect to Q_β^{-1} for a given period T and radius r can be expressed as

$$\frac{\partial C_R}{\partial Q_\beta^{-1}} = \frac{\partial C_R}{\partial Q_R^{-1}} \frac{\partial Q_R^{-1}}{\partial Q_\beta^{-1}}, \tag{2.8}$$

where

$$\frac{\partial Q_R^{-1}}{\partial Q_\beta^{-1}} = \frac{2L}{C_R} \frac{\partial C_R}{\partial L} + \frac{8}{3} \frac{L}{A} \left(\frac{A}{C_R} \frac{\partial C_R}{\partial A} \right). \tag{2.9}$$

L and A are the elastic moduli associated with V_{SV} and V_{PH}. The relation (2.9) is strictly valid for an isotropic medium for which $L = \mu$ and $A = \lambda + 2\mu$, but the extension to radial anisotropy is straightforward (Dziewonski & Anderson 1981). However, we do not have sufficient resolution in the data to distinguish between Q_L^{-1} and Q_N^{-1} or between Q_A^{-1} and Q_C^{-1}.

$$\frac{\partial C_R}{\partial Q_\beta^{-1}} = \frac{2C_R}{\pi} \ln \frac{T_0}{T} \left[\frac{L}{C_R} \frac{\partial C_R}{\partial L} + \frac{4}{3} \frac{L}{A} \left(\frac{A}{C_R} \frac{\partial C_R}{\partial A} \right) \right]. \tag{2.10}$$

Now

$$\frac{1}{C_R} \frac{\partial C_R}{\partial Q_\beta^{-1}} = -\frac{1}{T} \frac{\partial T}{\partial Q_\beta^{-1}}, \tag{2.11}$$

so that for spheroidal modes

$$\frac{\partial T}{\partial Q_\mu^{-1}} = \frac{1}{\pi} \ln \frac{T_0}{T} \left(L \frac{\partial T}{\partial L} + \frac{4}{3} L \frac{\partial T}{\partial A} \right). \tag{2.12}$$

A comparable set of equations can be found for Love waves (or toroidal modes).

2.3 The inverse problem

In any inverse problem the choice of parametrization is very important. As discussed above we work with a parameter space of seven physical quantities: ρ, Q_μ^{-1}, V_{PH}, V_{SV}, ξ, ϕ, η defining a radially anisotropic medium as a function of radius r. Within the mantle we have adopted a polynomial representation of the physical parameters over six depth ranges: 18–220 km (lithosphere–low-velocity zone), 220–410 km, 410–660 km (upper transition zone), 660–1000 km (lower transition zone), 1000–2680 km (lower mantle), 2680–2890 km (D″-layer). Continuity of the parameters is forced at 220 km and 1000 km to avoid the introduction of discontinuities at those depths. In addition, the density distribution is required to be compatible with the mass and moment of inertia of the earth, which imposes two integral constraints on density ρ (see Appendix A).

In each layer H_k lying between $r_{\inf}$ and $r_{\sup}$ the physical parameters $P_i^H(r)$ are expanded up to cubic polynomials:

$$P_i^H(r) = p_{0i} + p_{1i}\left(\frac{r-r_H}{\Delta_H}\right) + p_{2i}\left(\frac{r-r_H}{\Delta_H}\right)^2\left[+p_{3i}\left(\frac{r-r_H}{\Delta_H}\right)^3\right], \tag{2.13}$$

where r_H is a reference radius within the layer H, and $\Delta_H = r_{\sup} - r_{\inf}$ is the thickness of the layer. The cubic term is not included in all layers but only where continuity conditions are applied at one interface, which is the case at 220 km and 1000 km depths. The presence of the higher-order polynomial is justified in the first layer, where rapid variations in parameters can take place, and also in the lower mantle, which is by far the thickest layer and for which more degrees of freedom are desirable. The implementation of the continuity conditions is described in Appendix B, and with the imposition of these conditions we have the same number of free coefficients in each layer, which is very convenient for practical implementation.

The number of discrete parameters is equal to the product of six layers by seven physical parameters by three polynomial coefficients. When we allow for the two integral conditions on density we have 124 independent parameters. The approach is similar to that employed by Montagner & Anderson (1989b) but has been extended to greater depths with a generalization of the parametrization. The present inversion has been confined to the mantle, since the largest differences between body-wave and normal-mode models occur in this region. The procedure could easily be extended to include core structure in future work. With the polynomial representation of the physical parameters, the perturbations in the eigenperiod $\delta_n T_l$ due to parameter changes can be represented explicitly as

$$\delta_n T_l = \sum_{i=1}^{7}\sum_{k=1}^{k=N_H}\sum_{j=1}^{n_H} p_{ji}^k \int_{r=r_{k_{\inf}}}^{r=r_{k_{\sup}}} \left(\frac{\partial_n T_l}{\partial P_i}\right)\left(\frac{r-r_{H_k}}{\Delta_{H_k}}\right)^j \frac{dr}{\Delta h}, \tag{2.14}$$

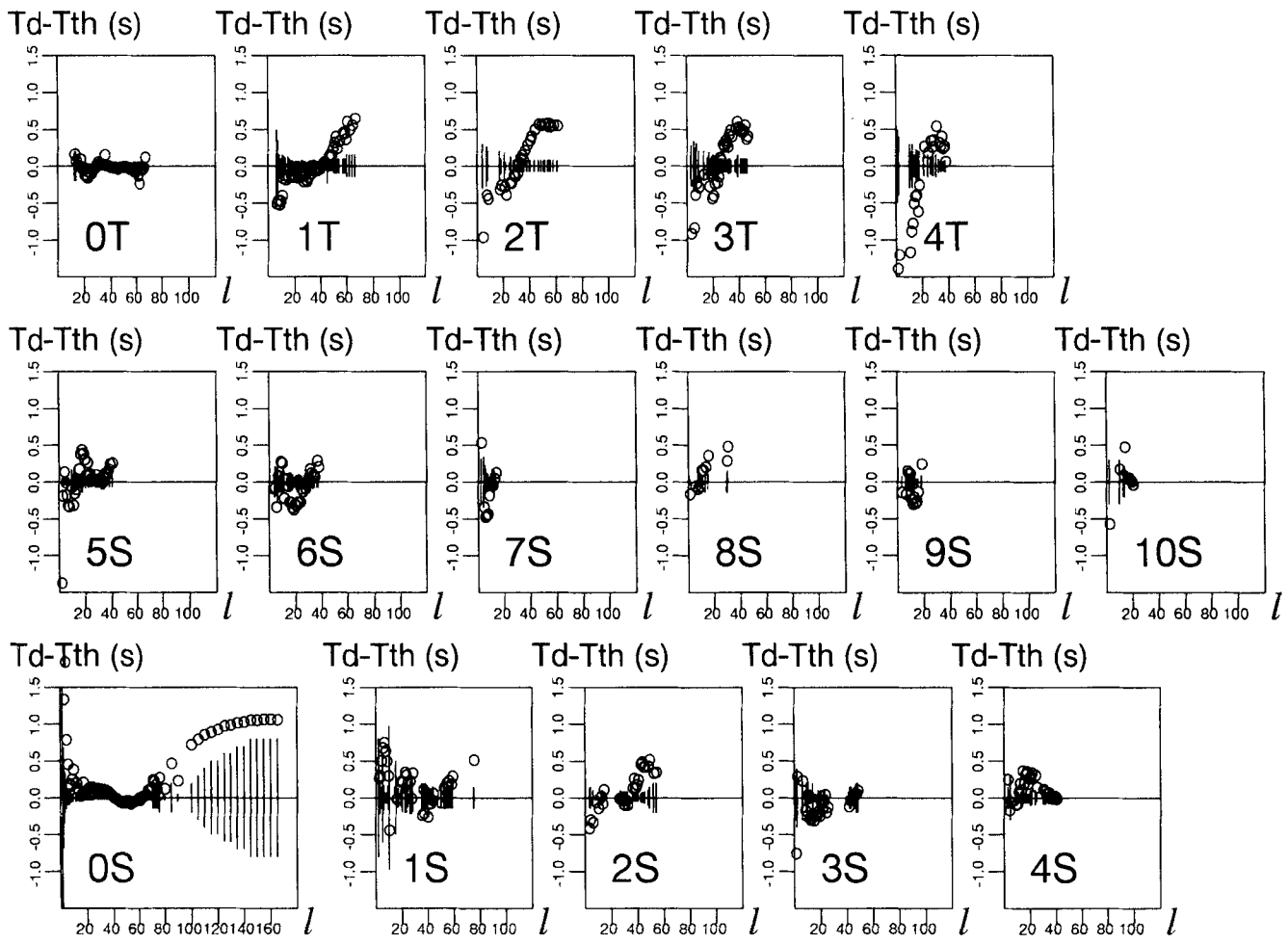

Figure 5. Eigenperiod residual display, as in Fig. 1, for *ak135-Q* after inversion for attenuation and density.

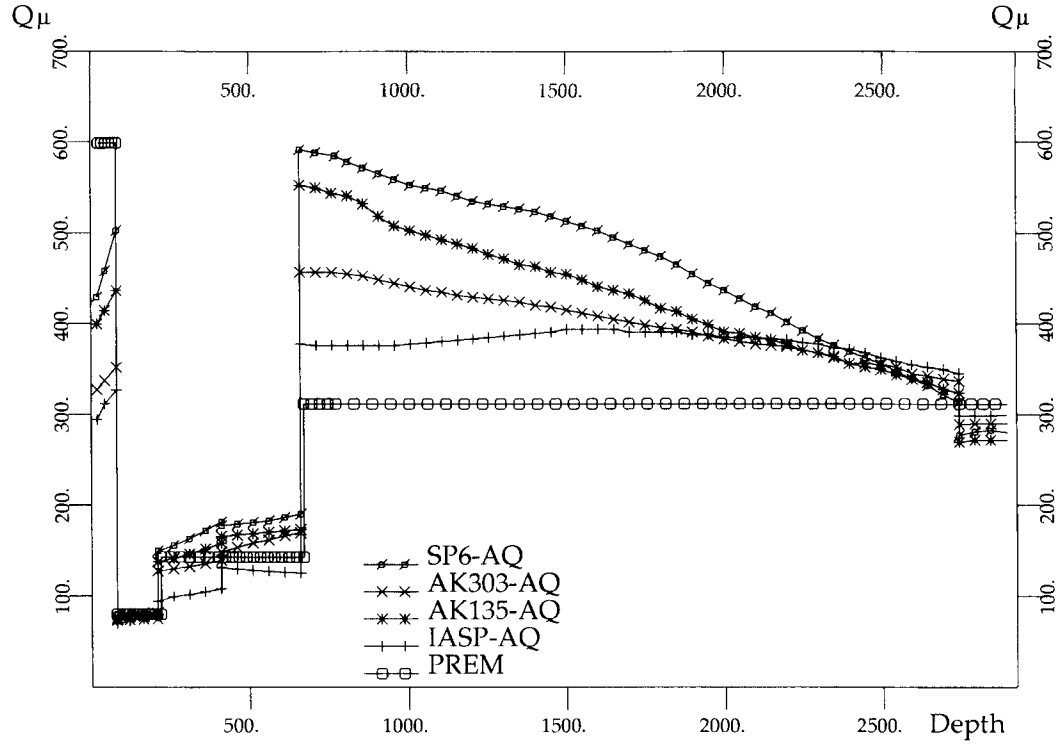

Figure 6. Attenuation models, Q_μ, for inversions where attenuation, density and the anisotropic parameters ξ, ϕ and η are allowed to vary.

where N_H is the number of depth ranges and n_H is the number of polynomial coefficients in layer H_k.

We can express the forward problem of calculating the eigenperiods for a given set of parameters in a formal way as

$$\mathbf{d} = \mathbf{g}(\mathbf{P}), \tag{2.15}$$

where $\mathbf{g}$ is a non-linear functional of the parameters $\mathbf{P}$. In this formulation we can use the algorithm of Tarantola & Valette (1982) to generate an improved parameter estimate $\mathbf{P}_f$ from an initial parameter distribution $\mathbf{P}_0$:

$$\mathbf{P}_f - \mathbf{P}_0 = (\mathbf{G}^T\mathbf{C}_d^{-1}\mathbf{G} + \mathbf{C}_p^{-1})^{-1}\mathbf{G}^T\mathbf{C}_d^{-1}[\mathbf{d} - \mathbf{g}(\mathbf{P}) + \mathbf{G}(\mathbf{P} - \mathbf{P}_0)]. \tag{2.16}$$

Here $\mathbf{C}_d$ is the data covariance matrix, $\mathbf{C}_p$ the covariance matrix for the parameters $\mathbf{P}$, and the kernels $\mathbf{G}$ are given in Takeuchi & Saito (1972) and Dziewonski & Anderson (1981).

The parameter covariance function $\mathbf{C}_p$ between parameters p_1 and p_2 at radii r_i and r_j is defined as

$$\mathrm{Cov}_{p_1,p_2}(r_i, r_j) = \sigma_{p_1}\sigma_{p_2}\,\mathrm{Cor}_{p_1,p_2}\exp - \left(\frac{r_i - r_j}{2H_{r_i}H_{r_j}}\right)^2, \tag{2.17}$$

where Cor_{p_1,p_2} is the correlation between the physical parameters p_1 and p_2, inferred for example from petrological models (Montagner & Anderson 1989a), and L_{r_i}, L_{r_j} are radial correlation lengths which enable us to smooth the model produced in the inversion. The linearized resolution matrix $\mathbf{R}$ can be derived from (2.16) as

$$\mathbf{R} = (\mathbf{G}^T\mathbf{C}_d^{-1}\mathbf{G} + \mathbf{C}_p^{-1})^{-1}\mathbf{G}^T\mathbf{C}_d^{-1}\mathbf{G}. \tag{2.18}$$

For our class of slightly non-linear problems we apply the Tarantola & Valette algorithm (2.16) in an iterative manner to improve the match to the observed eigenperiods.

2.4 Initial models

A number of different reference models for seismic wavespeeds derived from body-wave observations have been used as starting models for the inversion.

In addition to *iasp91* (Kennett & Engdhal 1991) and *sp6* (Morelli & Dziewonski 1993) two new models, *ak303* and *ak135* (Kennett *et al.* 1996), are used. These new velocity models have been constructed to provide an improved fit to smoothed empirical traveltimes for a wide variety of phases. These empirical times were derived from the ISC arrival-time catalogue after event relocation using P readings with the *iasp91* model (Kennett *et al.* 1996). This process has revealed some limitations in the earlier models, notably in the consistency of P- and S-wave times. The *iasp91* model has a 1 s baseline shift for S, which is reduced to 0.5 s for *sp6* and reduced to less than 0.1 s for *ak303* and *ak135*. Since the normal-mode periods are very sensitive to the S-wavespeed distribution, we can anticipate some differences in the character of the inversions for the different starting models.

Each of the body-wave models has an associated continental crust, and a modest adjustment was made to include a globally averaged crustal model before the inversion process for the eigenperiod data was begun.

3 RESULTS OF THE INVERSION EXPERIMENTS

3.1 Inversion for Q_μ and ρ

In this first experiment we attempt to match the eigenfrequency data set by only inverting for Q_μ and ρ. The velocity distributions V_P and V_S are fixed and the anisotropic parameters

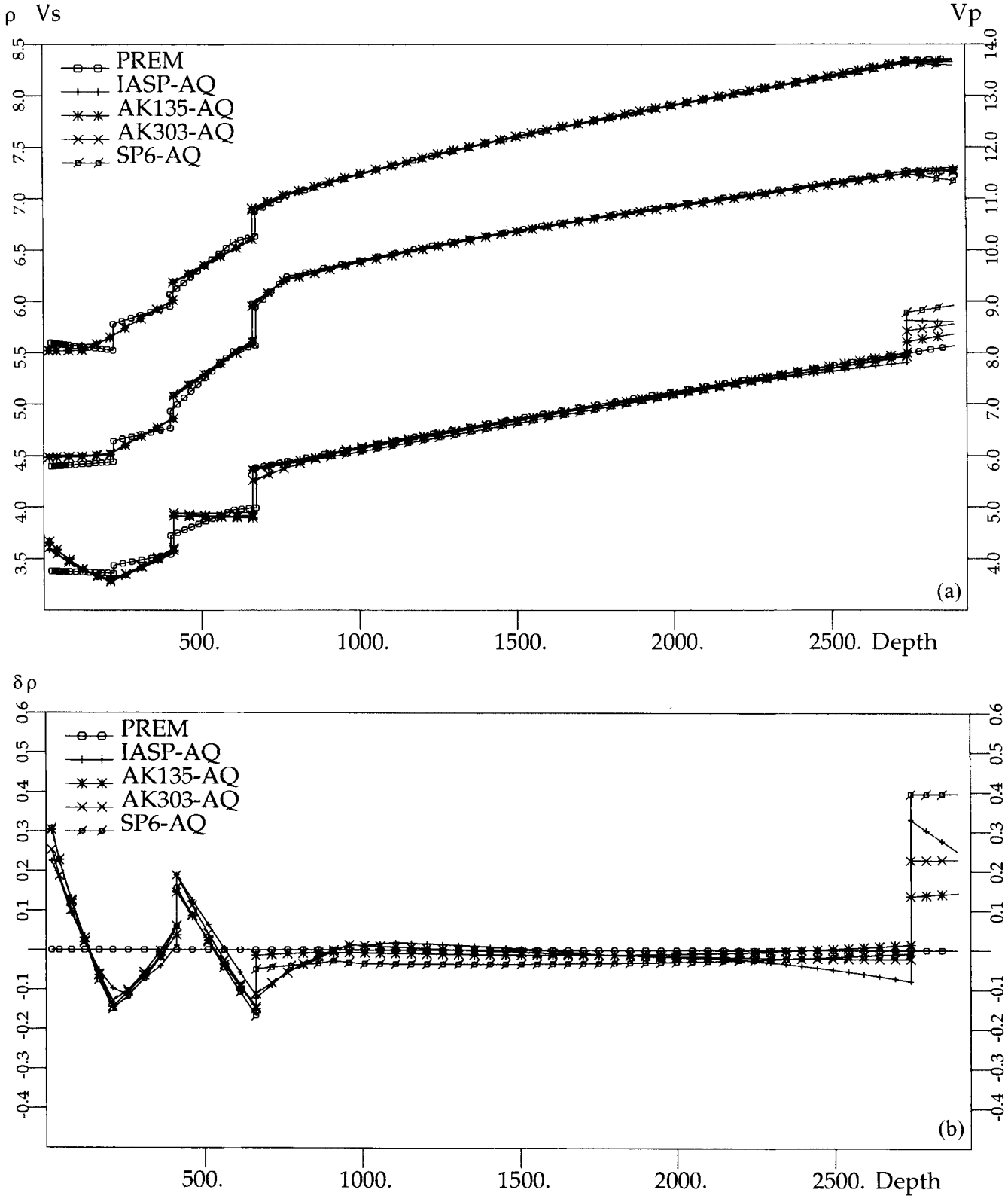

Figure 7. Density models. (a) Absolute values, (b) $\delta\rho$ in inversion for attenuation, density and anisotropic parameters.

ξ, ϕ, η are all set equal to unity. The results of the inversions are displayed in Figs 3 and 4. In the upper panel of each of these figures we display the starting models and in the lower panels the outcome of the inversion.

The attenuation results are shown in Fig. 3 and irrespective of the starting model there is an increase in Q_μ in the lower mantle, but there is considerable variability in the detailed distribution, particularly with respect to the gradients of Q_μ.

We can conclude that Q_μ needs to be increased in the lower mantle from the *prem* value, but that its variation with depth is poorly constrained. In the upper mantle between 80 km (the base of the lithosphere) and 660 km, perturbations in Q_μ away from the starting model are quite small. However, in the lithosphere itself, Q_μ ranges from 300 to 600 depending on the velocity model and is evidently weakly constrained by the eigenperiod data.

The density results are displayed in Fig. 4. The perturbations of ρ are shown in Fig. 4(b) and are large in the upper mantle, the lower transition zone and the base of the lower mantle (D″-layer). The large negative gradient in density in the first

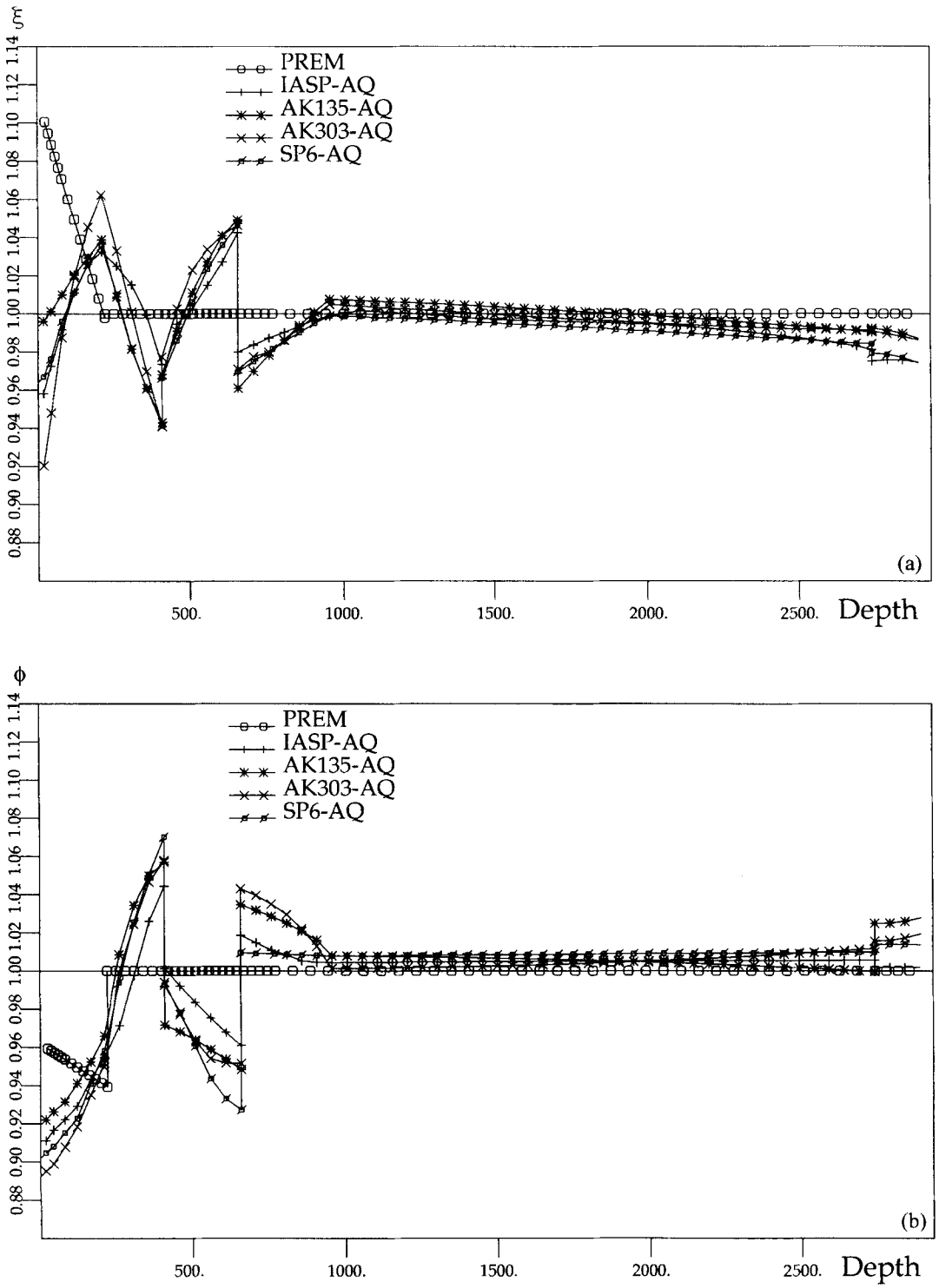

Figure 8. Anisotropic parameters inversion for Q_μ, ρ, ξ, ϕ and η. (a) ξ, the *S*-wave anisotropy; (b) ϕ, the *P*-wave anisotropy; (c) anisotropic parameter η.

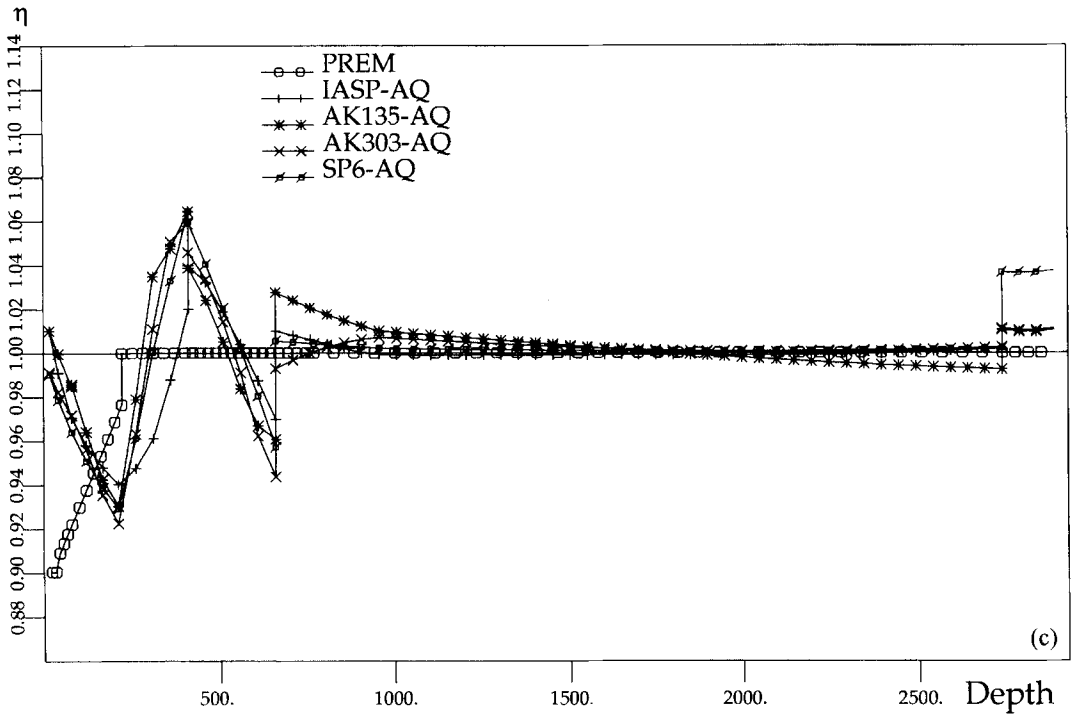

Figure 8. (*Continued.*)

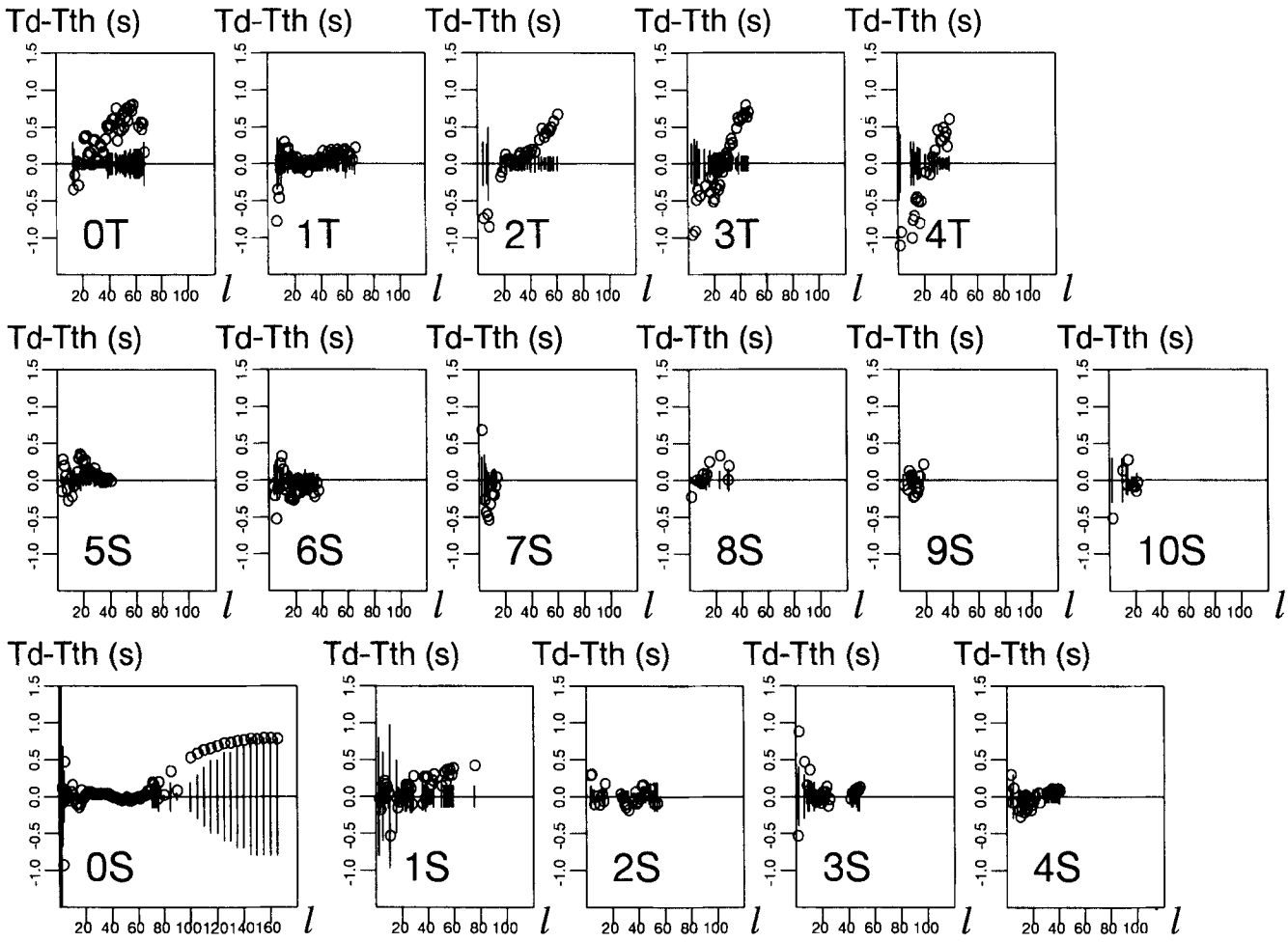

Figure 9. Eigenperiod residual display as in Fig. 1, for *ak135-AQ* after inversion for Q_μ, ρ, ζ, ϕ and η.

220 km is probably induced by the absence of a low-velocity zone in the starting models. Montagner & Anderson (1989b) have shown that a low-velocity zone makes it easier to explain normal modes that are sensitive to the upper mantle. Since we have assumed V_S to be fixed,

$$\delta V_S = \frac{1}{2}\left(\frac{\delta\mu}{\mu} - \frac{\delta\rho}{\rho}\right) = 0, \tag{3.1}$$

and so a positive $\delta\mu$ will be automatically compensated by an

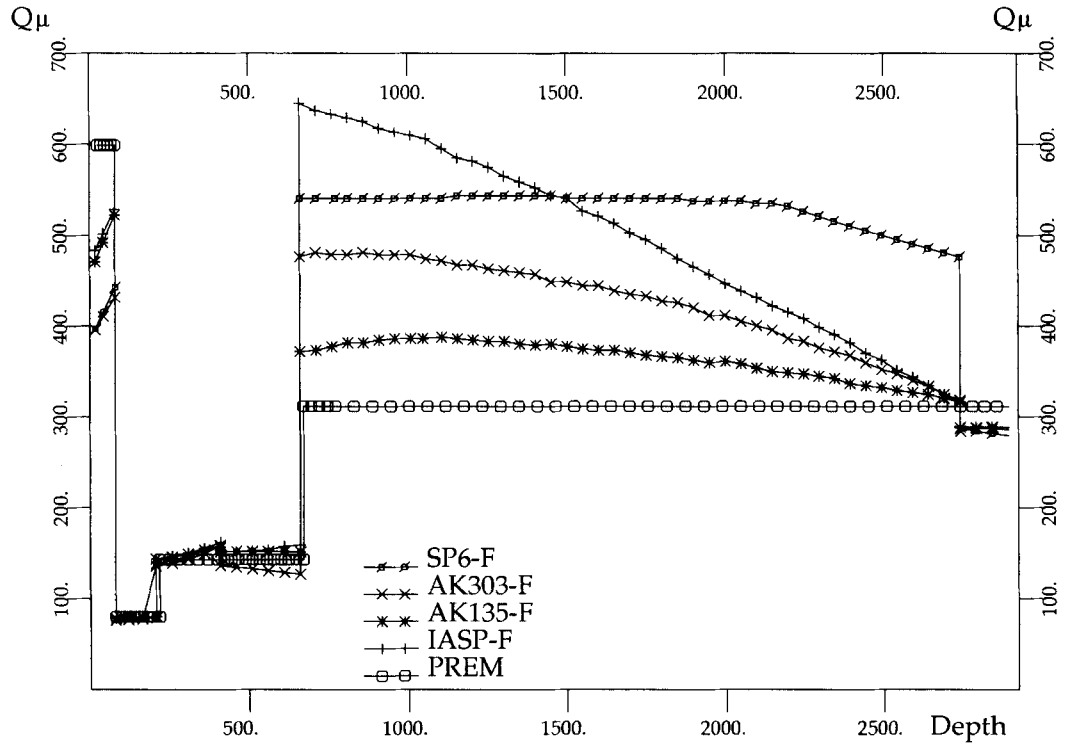

Figure 10. Free inversion for all seven parameters Q_μ, ρ, ξ, ϕ, η, V_P and V_{SV}: Q_μ attenuation models.

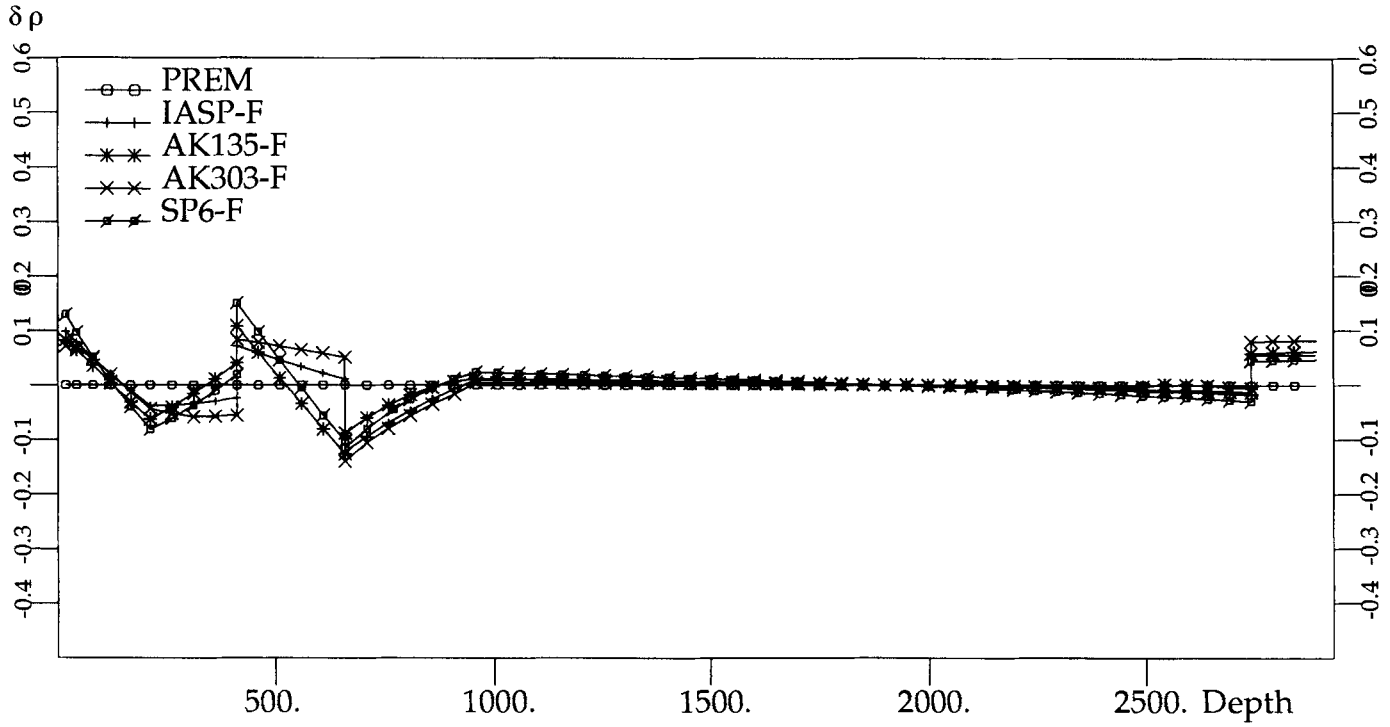

Figure 11. Free inversion for all seven parameters: density perturbations from starting models.

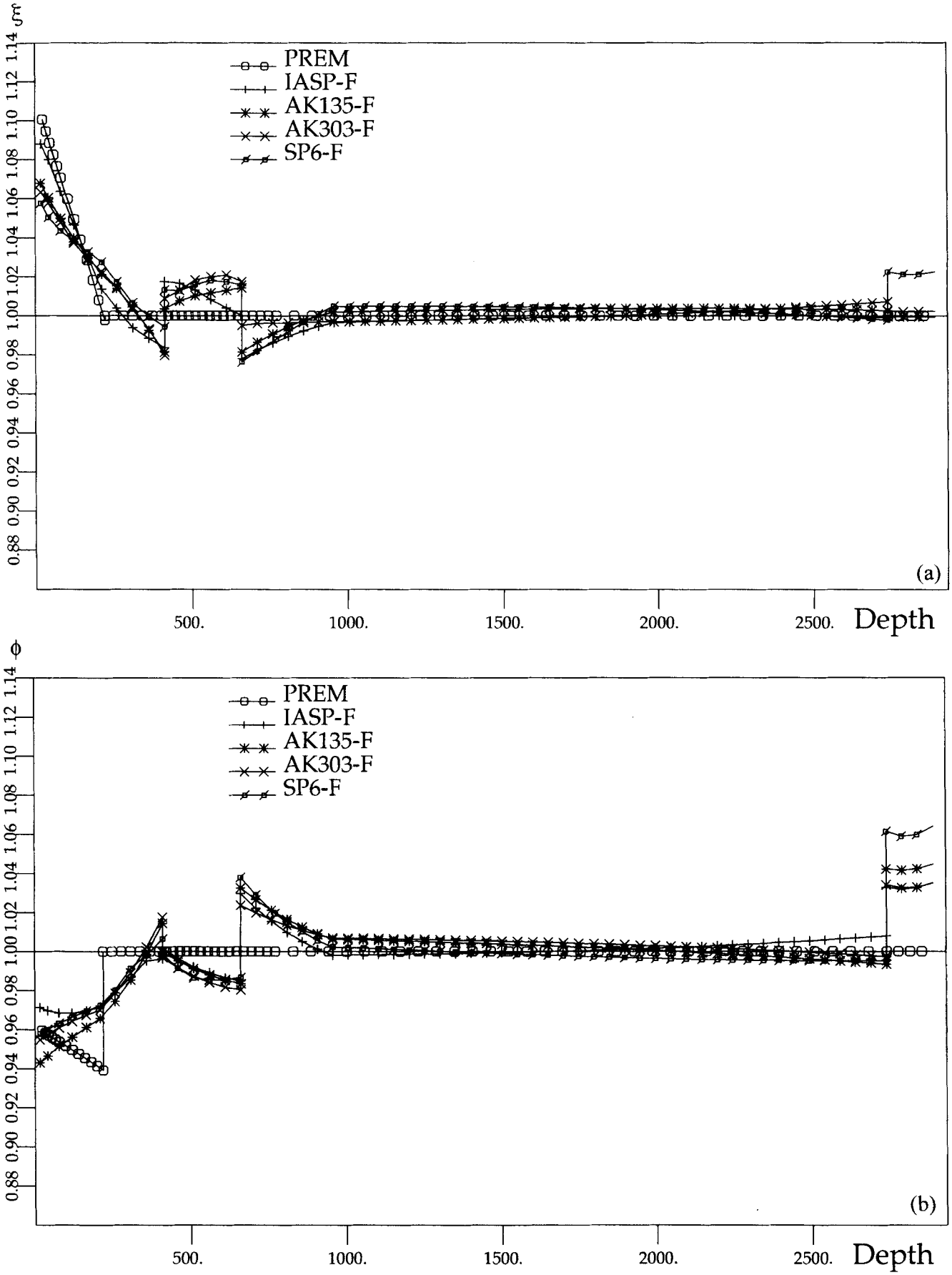

Figure 12. Anisotropic parameter after inversion for all seven parameters. (a) ξ, the *S*-wave anisotropy; (b) ϕ, the *P*-wave anisotropy; (c) anisotropic parameter η.

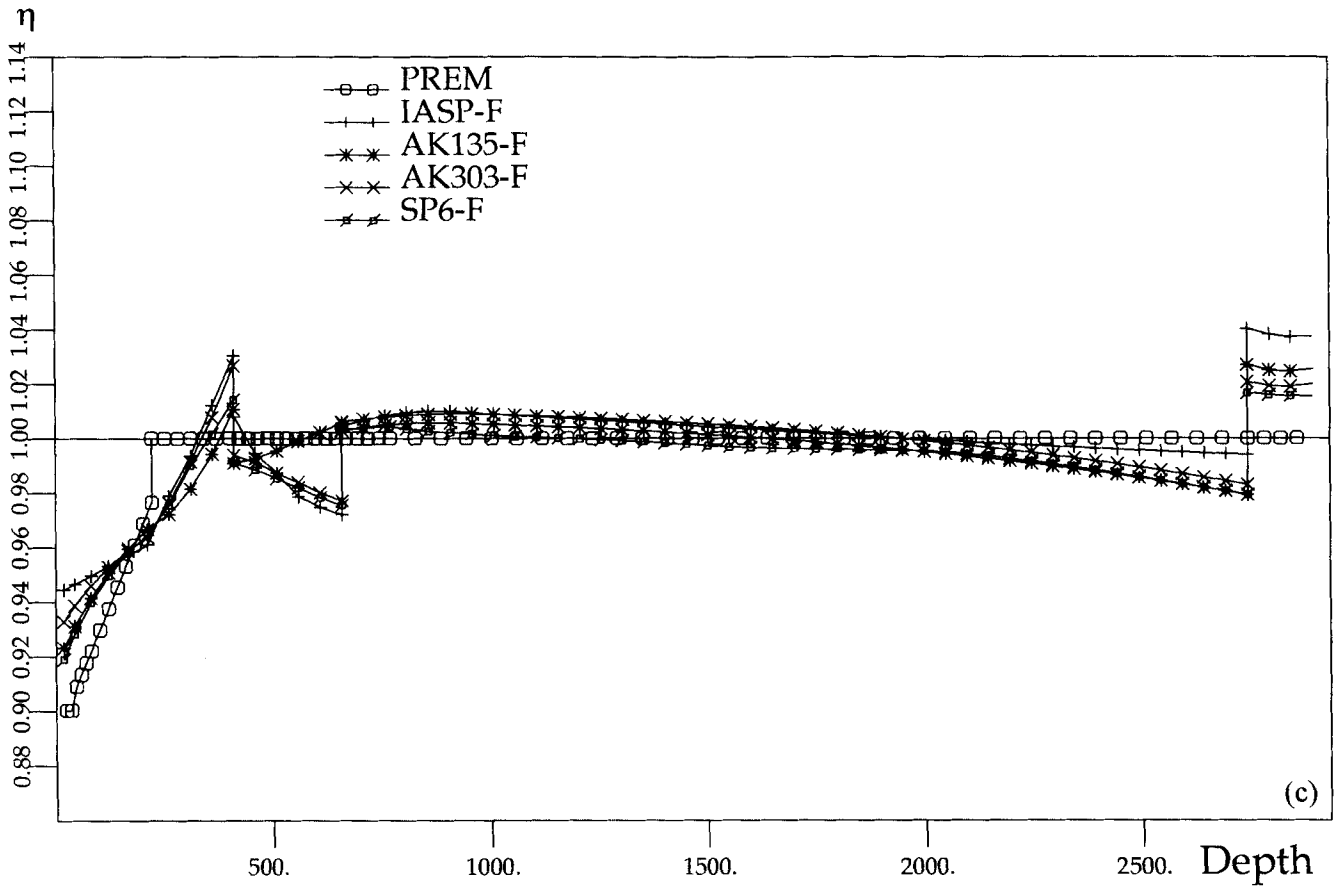

Figure 12. (*Continued.*)

equivalent $\delta\rho$. Therefore, the reversed gradient of density in the upper 220 km might be an artefact of our models.

For the other depth ranges, however, we can be more confident that the velocity models are close to a global average and so the density results can be interpreted directly. A robust feature of the inversions is an increase in the density jump at the 410 km discontinuity, and a slight decrease in the jump at the 660 km discontinuity accompanied by lowered densities in the lower transition zone (660–1000 km). In this zone, the density gradient is no longer consistent with the Adams–Williamson equation for a self-compressed model, and this suggests important mineralogical variations in this depth range. There is also a tendency for increased density compared with the starting models for D″, reflecting the complexity of this layer.

After these inversions, most of the discrepancy between observed and calculated eigenperiods has been removed, but even so many eigenperiods are not satisfactorily explained and the misfit χ is of the order of 3–4 for all the final models. Fig. 5 shows the eigenperiod residuals for *ak135-Q*. There is some offset for the fundamental spheroidal modes associated with shallow structure, and significant discrepancies for higher-order toroidal modes, which is not surprising since it is well known that some amount of anisotropy is necessary to explain both spheroidal and toroidal modes simultaneously.

3.2 Inversion for Q_μ, ρ and anisotropic parameters

In this second experiment we release the constraints on ξ, ϕ and η. The starting models used were those derived in the previous experiment. An alternative inversion was performed using the original starting models (*iasp91*, *ak135*, *ak303*, *sp6*) but this made little difference to the final models. All perturbations are displayed with respect to these starting models.

The attenuation and density models are only slightly affected by allowing radial anisotropy. For Q_μ (Fig. 6), there is an improved consistency between the different inversions in the lower mantle, with an average value around 360, but still a broad span in the lower transition zone. In the uppermost mantle, there is now less variability between models with Q_μ in the range 300–500. The density variations (Figs 7a, b) are quite similar to the previous results in Fig. 4, except that the decrease in density in the lower transition zone is rather weaker and there is only a slight decrease in the density jump at 660 km for most of the models. Once again, all the inversions show a significant increase in density from *prem* in the D″-layer.

The three classes of anisotropic parameters determined from the eigenperiod inversions are plotted in Fig. 8. The most striking feature is the difference between the upper mantle and the lower mantle. In the upper mantle, the three anisotropic parameters differ significantly from the isotropic value of unity and display a succession of large gradients. The difference between the inverse gradient of radial anisotropy in the first 220 km and that for *prem* is striking. Radial anisotropy is large (several per cent) in these models not only in the top 220 km but also in the upper transition zone. The reversed anisotropy between 220 and 410 km suggests that flow in this depth range is primarily radial as compared with that in the uppermost

mantle and upper transition zone where horizontal motion explains the style of anisotropy.

An important result is that the anisotropy in the bulk of the lower mantle is very small, as was also found for the *core11* model of Widmer (1991). There is some indication of radial anisotropy in the lower transition zone, but with an amplitude smaller than in the upper mantle. The behaviour in the D″-layer is more complex, with small *S*-wave anisotropy (Fig. 8a) but larger *P*-wave and η anisotropies (Figs 8b and 8c). This kind of behaviour is difficult to explain with petrological models, and a new mechanism might be needed to explain this style of anisotropy. However, we cannot rule out a possible trade-off between the anisotropic parameters and the seismic velocities due to the limitations of the starting models. It is interesting to note that model *sp6* with the strongest velocity gradients in D″ leads to the largest η anisotropy.

The residuals for the eigenperiod data are displayed in Fig. 9 for the radially anisotropic model derived from *ak135* with the inclusion of Q. This model provides a good fit to body-wave information and also gives a satisfactory match to most eigenperiods, with a misfit measure χ of the order of 2. Similar results are obtained for the other starting models. Compared with Fig. 5, which displays the eigenperiod residuals without inclusion of anisotropy, we note that the residuals in Fig. 9 for the fundamental spheroidal modes ($_0S$) and first-order toroidal modes ($_1T$) are reduced, but the fit to the fundamental toroidal modes ($_0T$) has actually become worse.

3.3 Inversion for the whole set of parameters

In this last inversion experiment all seven parameters are allowed to vary, so that we relax the constraints on V_P and V_S. A number of differences can be noticed compared with the previous results; in particular, the amplitude of the perturbations is somewhat smaller. The absolute values of Q_μ (Fig. 10) are mostly lower than in the previous cases, but even so Q_μ is significantly larger than in the *prem* or *core11* models. The perturbations in density ρ (Fig. 11) are very similar to the previous cases, with a small gradient in density in the upper transition zone, a slight decrease in density from the original models in the lower transition zone, and an increase in the D″ layer.

The most important changes occur for the anisotropic parameters (Fig. 12a–c). Once all the parameters are allowed to vary, all the anisotropic parameters display the same general character as *prem* and *core11* in the uppermost 210 km. There is clearly a significant trade-off between the anisotropic parameters and the *S* and *P* wavespeeds. Radial anisotropy is still present in the upper transition zone, but compared with the previous inversions there is a different gradient and a smaller amplitude. However, the low level of radial anisotropy in the bulk of the lower mantle, and the significant anisotropy in the lower transition zone and D″ are robust features of all the inversions.

The velocity and density profiles produced from the different starting models are generally consistent except in the upper

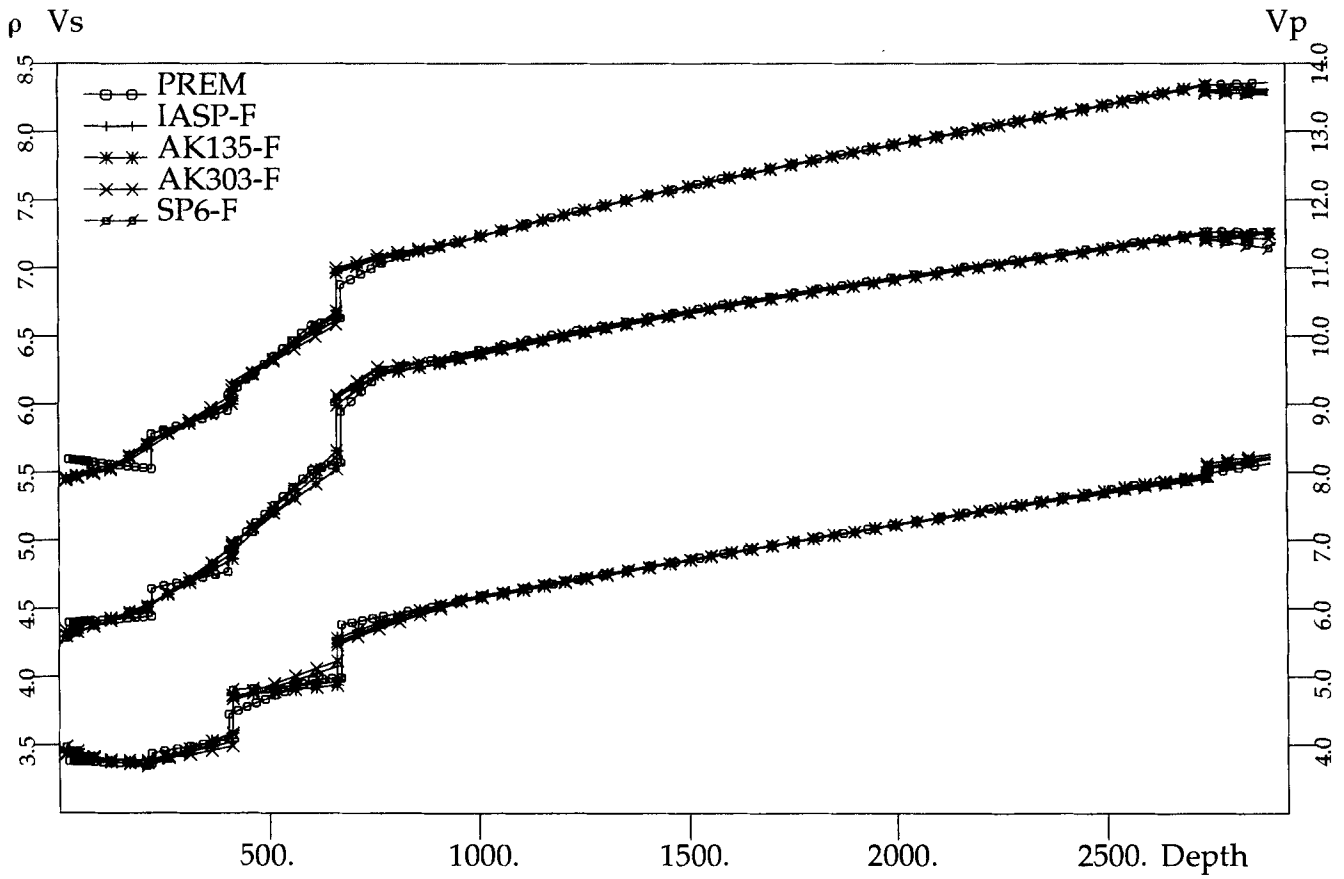

Figure 13. Free inversion for all seven parameters: velocity and density profiles.

transition zone and D″ (Fig. 13). The inclusion of the extra degrees of freedom markedly improves the level of fit between observed and computed eigenperiods, and the final models have a misfit χ close to 1. The residuals of the eigenperiods for model *ak135-f*, obtained from an inversion with *ak135* and the *premQ* model as a starting point, are displayed in Fig. 14. The majority of the eigenperiods are now fit to within their standard errors and the fits to the toroidal-mode eigenfrequencies are markedly improved. However, we have adjusted the V_S and V_P profiles and so have modified the traveltimes for the models. Although we have reduced the eigenperiod misfit significantly, we have produced the opposite effect on the traveltimes, and now, for example, the traveltime misfit measure for the 18 major phase branches for *ak135-f* is over 12 compared with 4.4 for the original model *ak135*.

4 DISCUSSION

4.1 Robust features of the inverse models

The range of experiments reported in the previous sections enables us to display a number of robust features of the inverse models with respect to attenuation, density and radial anisotropy.

The influence of the attenuation profile is very large, but, unfortunately, the currently available data do not provide strong constraints. The Q_μ models have been derived from the dispersive properties of seismic velocities rather than directly from attenuation data. Nevertheless, as we shall see in the next section, our models are in agreement with the normal-mode attenuation data reported by Okal & Jo (1990) and Widmer (1991). The most robust feature of the attenuation profiles is a significant increase in Q_μ relative to the *prem* or *core11* models, with values above 400 for most of the lower mantle, except D″. Our inversions also favour lower Q than for *prem* in the lithosphere, with Q_μ between 400 and 500.

The density results indicate clear trends in perturbations from the *prem* base model. There is a need for an increase in density in D″, a decrease in the lower transition zone (660–1000 km depth), an increase in the density jump at the 410 km discontinuity, and a slight decrease in the density jump at the 660 km discontinuity. These variations in density may be indicative of radial inhomogeneity in composition, both in the transition zone and in the D″-layer.

Radial anisotropy is not required in most of the lower mantle except in the boundary layers (lower transition zone and D″). In no case was the deviation of the anisotropic parameters from unity significant. However, radial anisotropy was quite large in the top 220 km, but the gradients were poorly constrained. If such radial anisotropy is present in the upper and lower transition zones it is much smaller than in the uppermost layer. The anisotropy in D″ is of a very different

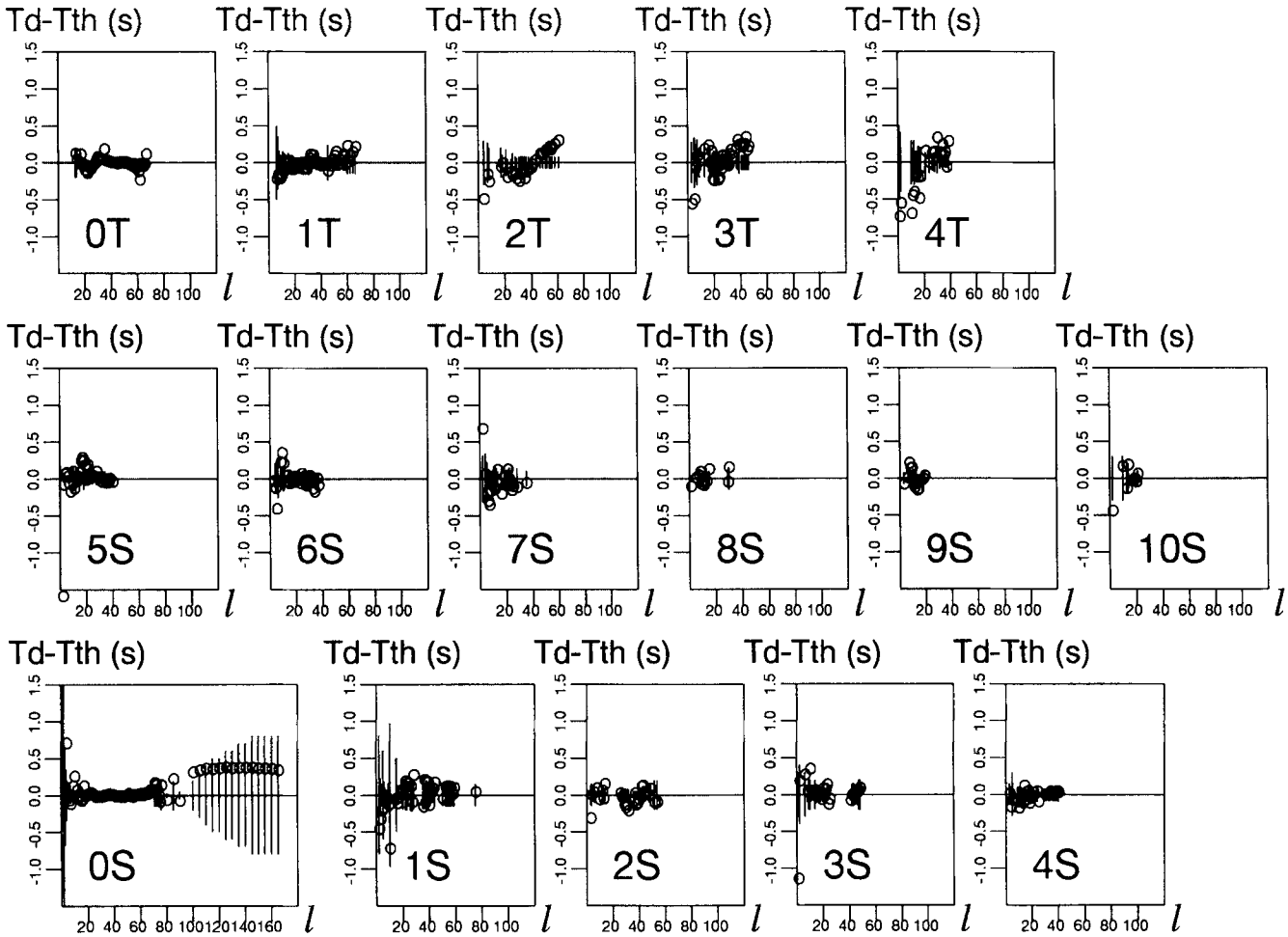

Figure 14. Eigenperiod residual display as in Fig. 1, for *ak135-f* after inversion for all seven parameters.

nature: it is small for V_S but large in V_P and η, which suggests that a special mechanism needs to be found, possibly by some coupling with the core.

4.2 Comparison with attenuation data

The inverse models we have constructed can be used to calculate the attenuation of normal modes for comparison with the available normal-mode attenuation data. Widmer (1991) has made a compilation of such attenuation results; most of this data set is composed of quality factors for fundamental modes, so it is not surprising that resolution in the lower mantle is poor. However, he omitted some overtone data obtained by Okal & Jo (1990). Moreover, the errors associated with measurements of normal-mode Q are very large, because it is difficult to unravel from amplitude measurements the competing influences of physical attenuation and lateral heterogeneity (which produces focusing and defocusing as well as scattering).

We have therefore compared the ${}_nQ_l$ estimates for the model *corell* with our calculated values (see Fig. 15). An error estimate of 10 per cent was assigned to each Q value; this probably represents an overestimate for the fundamental modes and an underestimate for the other modes. However, these error bars give a rough indication of what we can expect and allow a rapid comparison between two models. We find that, although the Q models are quite different, the residuals between the ${}_nQ_l$ estimates are rather small, and mostly smaller than the assigned error bars. Our approach for retrieving Q_μ, although somewhat artificial and indirect, turns out to be consistent with the data. Therefore, we conclude that our models do not display abnormal normal-mode quality factors, despite high values of Q_μ in the lower mantle. Our results are in complete agreement with previous results by Okal & Jo (1990) concerning Q_μ in the lower mantle.

We have made a number of assumptions in the attenuation study that need to be examined more closely. First, we did not try to invert for Q_κ, which was assumed to be infinite, and second we assumed that Q_μ is independent of frequency. Both of these hypotheses are probably wrong, but currently there are no data available to reveal their shortcomings. It is highly desirable that improved data acquisition be carried out for attenuation studies so that greater insight can be gained into the attenuation processes of seismic waves and normal modes.

5 CONCLUSIONS

We have been able to demonstrate that we can achieve a reconciliation between models derived from high-frequency

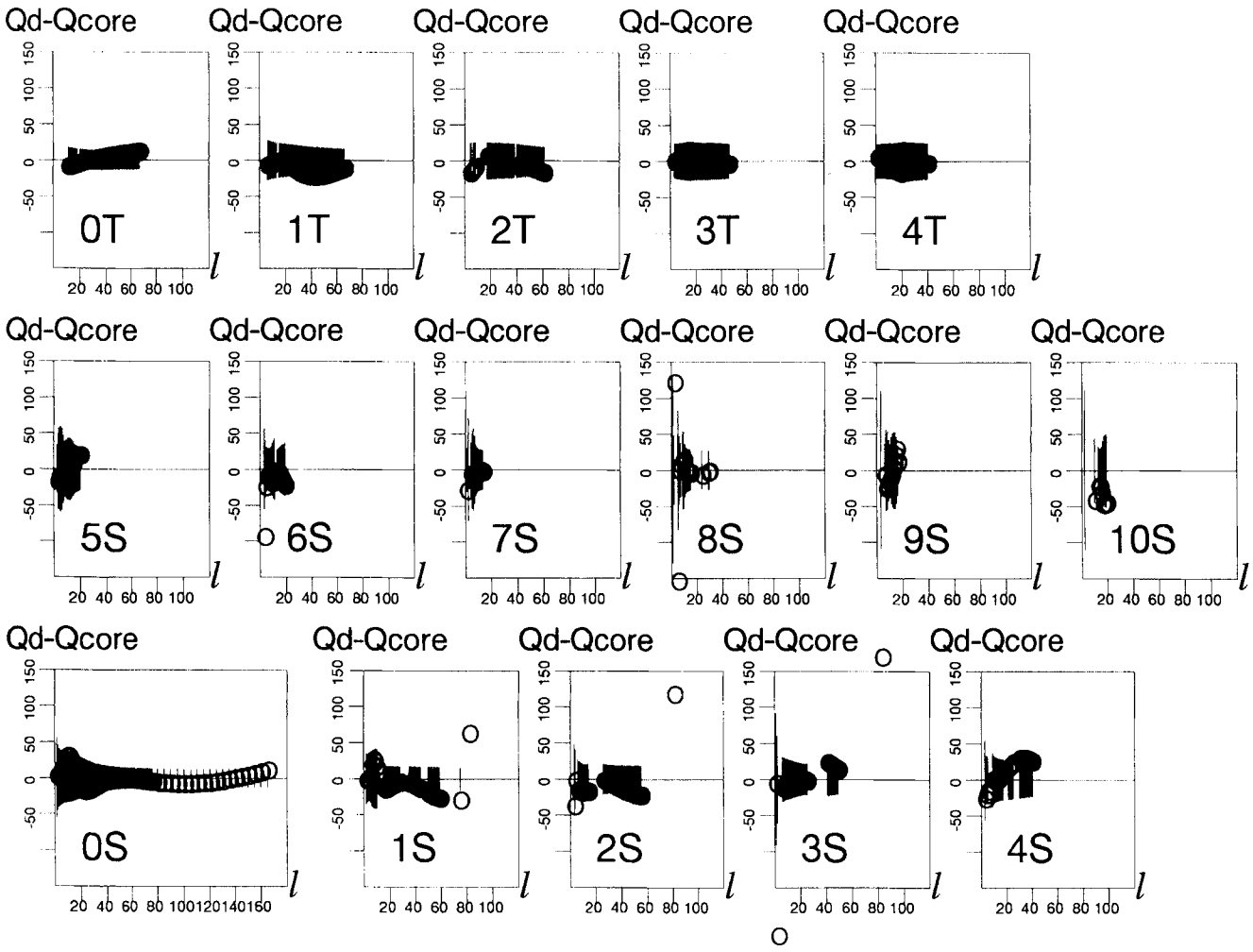

Figure 15. Residuals for modal attenuation factors ${}_nQ_l$ for the models *corell* and *ak135-f*.

body-wave and normal-mode data by including the dispersive influence of attenuation and a density model. The attenuation and density profiles show some differences from those models derived directly from normal-mode observations, with enhanced Q_μ in the lower mantle and some adjustment in the densities through the transition zone and D″-layer.

The fit between the estimated observed normal-mode eigenperiods can be improved somewhat by allowing radial anisotropy in the model (i.e. transverse isotropy with a vertical symmetry axis). The extra degrees of freedom improve the compatibility between spheroidal and toroidal modes, whilst retaining a good representation of body-wave information. The radial anisotropy is most significant in the shallower parts of the model and is not needed in the bulk of the lower mantle.

A very close fit can be obtained to the eigenperiod data by releasing the constraints on the V_P and V_S distributions previously imposed from the body-wave work and then performing a seven-parameter inversion. Once again, radial anisotropy is most significant in the shallower part of the model but the character is modified by trade-offs between the anisotropic parameters and velocity. However, the improved fit to the eigenperiods is achieved at the expense of a degradation of the representation of the traveltimes for major body-wave phases. The final models from these unconstrained inversions barely represent an adequate fit to the traveltimes and are nowhere near as good as the best of the original models.

We can therefore come very close to a reconciliation of models which represent the body-wave and normal-mode observations, using density and attenuation. We have to recognize that the optimum models for each class differ. However, the differences are very small except in the upper mantle.

Neither the global observations of normal modes, nor the continental biased observations of seismic arrival times provide an adequate basis for the representation of the outer layers of the Earth, which display the largest amounts of lateral heterogeneity. Normal-mode data will represent a combination of structures beneath oceanic and continental regions with a very different sampling from that with traveltime data. In any global model, there will therefore be some degree of artificiality in the shallow structure, and additional parameters such as radial anisotropy can help to reconcile the problems induced by lateral heterogeneity.

ACKNOWLEDGMENTS

This is an RSES contribution, and IPGP contribution 1386. This work was supported by Action Thématique Programmée Tomographie and a Visiting Fellowship from the Research School of Earth Sciences to J-P.

REFERENCES

Bussy, M., Montagner, J.P. & Romanowicz, B., 1993. Tomographic model of attenuation in the Pacific Ocean, *Geophys. Res. Lett.*, **20,** 663–666.

Dziewonski, A.M. & Anderson, D.L., 1981. Preliminary Reference Earth Model, *Phys. Earth planet. Inter.*, **25,** 297–356.

Gilbert, F., 1970. Excitation of the normal modes of the Earth by earthquake sources, *Geophys. J. R. astr. Soc.*, **22,** 223–226.

Gilbert, F. & Dziewonski, A.M., 1975. An application of normal mode theory to the retrieval of structural parameters and source mechanisms from seismic spectra, *Phil. Trans. R. Soc. Lond.* A, **278,** 187–269.

Kanamori, H. & Anderson, D.L., 1977. Importance of physical dispersion in surface wave and free oscillation problems: review, *Rev. Geophys. Space Phys.*, **15,** 105–112.

Kennett, B.L.N. & Engdahl, E.R., 1991. Traveltimes for global earthquake location and, phase identifications, *Geophys. J. Int.*, **105,** 429–465.

Kennett, B.L.N., Engdahl, E.R. & Buland, R., 1996. Constraints on seismic velocities in the Earth from travel times, *Geophys. J. Int.*, submitted.

Lee, W.B. & Solomon, S.C., 1979. Simultaneous inversion of surface-wave phase velocity and attenuation: Rayleigh and Love waves over continental and oceanic paths, *Bull. seism. Soc. Am.*, **69,** 65–95.

Liu, H.-P., Anderson, D.L. & Kanamori, H., 1976. Velocity dispersion due to anelasticity; implications for seismology and mantle composition, *Geophys. J. R. Astr. Soc.*, **47,** 41–58.

Montagner, J.P. & Anderson, D.L., 1989a. Anisotropy of petrological models. Constraints on elastic combinations inferred from petrological models, *Phys. Earth planet. Inter.*, **54,** 82–105.

Montagner, J.P. & Anderson, D.L., 19809b. Constrained reference mantle model, *Phys. Earth planet. Inter.*, **58,** 205–227.

Morelli, A. & Dziewonski, A.M., 1993. Body wave traveltimes and a spherically symmetric *P*- and *S*-wave velocity model, *Geophys. J. Int.*, **112,** 178–194.

Okal, E.M. & Jo, B.-G., 1990. Q measurements for phase X overtones, *Pageoph.* **132,** 331–362.

Revenaugh, J. & Jordan, T.H., 1991. Mantle layering for ScS reverberations 3. The upper mantle, *J. Geophys. Res.*, **96,** 19 781–19 810.

Ritzwoller, M., Masters, G. & Gilbert, F., 1986. Observations of anomalous splitting and their interpretation in terms of aspherical structure, *J. geophys. Res.*, **91,** 10 203–10 228.

Ritzwoller, M., Masters, G. & Gilbert, F., 1988. Constraining aspherical structure with low frequency interaction coefficients: Application to uncoupled multiplets, *J. geophys. Res.*, **93,** 6369–6396.

Roult, G., Romanowicz, B. & Montagner, J.P., 1990. 3-D upper mantle shear velocity and attenuation from fundamental-mode free oscillation data, *Geophys. J. Int.*, **101,** 68–80.

Smith, M.F. & Masters, G., 1989. Aspherical structure constraints from free oscillation frequency and attenuation measurements, *J. geophys. Res.*, **94,** 1953–1976.

Takeuchi, H. & Saito, M., 1972. Seismic surface waves, in *Methods in Computational Physics,* **11,** 217–295, Academic Press, New York, NY.

Tarantola, A. & Valette, B., 1982. Generalized non-linear inverse problems solved using the least-squares criterion, *Rev. Geophys. Space Phys.*, **20,** 219–232.

Valette, B., 1986. About the influence of pre-stress upon adiabatic perturbation of the Earth, *Geophys. J. R. Astr. Soc.*, **85,** 179–208.

Valette, B. & Lesage, P., 1992. Retrieving Mean Earth models (abstract), *Int. Symp. Ten Years of GEOSCOPE—Broadband Seismology.*

Widmer, R., 1991. The large-scale structure of the Deep Earth as constrained by free oscillations observations, *PhD thesis,* University of California, San Diego.

Widmer, R., Masters, G. & Gilbert, F., 1993. Spherically symmetric attenuation within the Earth from normal mode data, *Geophys. J. Int.*, **104,** 541–553.

APPENDIX A: HOW TO TAKE ACCOUNT OF THE MASS AND INERTIA CONDITIONS?

The mass of the Earth M and its moment of inertia I are relatively well known.

$$M = \int_0^a 4\pi\rho r^2\, dr = 5.974 \times 10^{24}\ \mathrm{kg}, \qquad \text{(A1)}$$

and

$$I = \int_0^a \frac{8}{3}\pi\rho r^4\, dr = 0.3308 Ma^2. \tag{A2}$$

Any perturbation in ρ must conserve M and I. In order to ensure these constraints, a variety of solutions can be proposed. First of all, we can consider M and I as additional data. This solution is easy to implement, but has the disadvantage of mixing two different varieties of data and destroying the homogeneity of the data set (by mixing apples and pears). A second solution is to try to take account of these conditions directly, which makes it possible to decrease the number of independent parameters. As in Appendix B, we consider only two layers.

$$dM = \int_0^b 4\pi r^2\, drp_1 + \int_0^b 4\pi r^2 x_1(r)\, drp_2 + \int_0^b 4\pi r^2 x_1^2\, drp_3 + \int_b^a 4\pi r^2\, drp_4 + \int_b^a 4\pi r^2 x_2(r)\, drp_5 + \int_b^a 4\pi r^2 x_2^2\, drp_6, \tag{A3}$$

which can be rewritten as

$$dM = \sum_{i=1}^{n_p} \tilde{M}_i p_i, \tag{A4}$$

and in the same way we can represent the variation of the moment of inertia as

$$dI = \sum_{i=1}^{n_p} \tilde{I}_i p_i. \tag{A5}$$

We can also write the perturbation of ${}_nT_l$ in a comparable form:

$$d_nT_l = \sum_{i=1}^{n_p} \tilde{G}_i p_i. \tag{A6}$$

We can, for instance, decide to eliminate parameters p_1 and p_2. First, let us consider the mass condition:

$$dM = 0 \Rightarrow p_1 = \sum_{i=2}^{n_p} \frac{-\tilde{M}_i}{\tilde{M}_1} p_i, \tag{A7}$$

and we can modify the expression for the perturbation of ${}_nT_l$ to

$$d_nT_l = \sum_{i=2}^{n_p} \left(\tilde{G}_i + \tilde{G}_1 \frac{-\tilde{M}_i}{\tilde{M}_1}\right) p_i. \tag{A8}$$

An interesting consequence of this expression is that it is also valid for $i = 1$. Therefore, with only a single condition, it is only necessary to modify the kernels of the different parameters by adding an additional term $\tilde{G}_1 - \tilde{M}_i/\tilde{M}_1$.

Let us now consider the second constraint on the moment of inertia, in order to get rid of p_2.

$$dT = \sum_{i=2}^{n_p} \tilde{G}'_i p_i, \tag{A9}$$

$$p_2 = -\sum_{i=3}^{n_p} p_i + \sum_{i=3}^{n_p} \frac{\tilde{I}_1}{\tilde{I}_2}\frac{\tilde{M}_i}{\tilde{M}_1} p_i + \frac{\tilde{I}_1}{\tilde{I}_2}\frac{\tilde{M}_2}{\tilde{M}_2} p_2. \tag{A10}$$

Finally,

$$p_2 = \sum_{i=3}^{n_p} -\frac{\tilde{I}_i\tilde{M}_1 - \tilde{I}_1\tilde{M}_i}{\tilde{I}_2\tilde{M}_1 - \tilde{I}_1\tilde{M}_2} p_i. \tag{A11}$$

This equation is again valid for $i = 1$. We can use this last expression on the ${}_nT_l$ and finally we obtain

$$d_nT_l = \sum_{\substack{i=1 \\ i\neq 2}}^{n_p} \tilde{G}' i p_i + \tilde{G}'_2 \left[\sum_{i;i\neq 2}^{n_p} -\frac{\tilde{I}_i\tilde{M}_1 - \tilde{I}_1 M_i}{\tilde{I}_2\tilde{M}_1 - \tilde{I}_1\tilde{M}_2} p_i\right]. \tag{A12}$$

After some straightforward calculations, an expression is found in which the summation can be performed from 1 to n_p:

$$d_nT_l = \sum_{i=1}^{n_p} \left(\tilde{G}_i + \tilde{G}_1\left(\frac{\tilde{M}_2\tilde{I}_i + \tilde{I}_2\tilde{M}_i}{\tilde{I}_2\tilde{M}_1 - \tilde{I}_1\tilde{M}_2}\right) + \tilde{G}_2\left(\frac{\tilde{M}_1\tilde{I}_i + \tilde{I}_1\tilde{M}_i}{\tilde{I}_1\tilde{M}_2 - \tilde{I}_2\tilde{M}_1}\right)\right) p_i. \tag{A13}$$

All these expressions are easy to program and therefore can be incorporated in the inversion code.

APPENDIX B: CONTINUITY OF PARAMETERS AT AN INTERFACE BETWEEN TWO LAYERS

Let us assume that the Earth is composed of two layers, the first lying between radii 0 and b and the second between b and a, so that the radius b is the boundary between the two layers. Let us assume as well that δ_nT_l is only dependent upon one physical parameter with perturbation in layer 1, $\delta P_1(r)$ and in layer 2, $\delta P_2(r)$. We expand these perturbations in polynomials up to degree two:

$$\delta P_1(r) = p_1 + x_1 p_2 + x_1^2 p_3, \qquad \delta P_2(r) = p_4 + x_2 p_5 + x_2^2 p_6, \tag{B1}$$

where $x_k = (r - r_{H_k})/\Delta H_k$, r_{H_k} is the reference radius in layer H_k and $\Delta H_k = r_{k_{\text{inf}}} - r_{k_{\text{sup}}}$ is the thickness of the layer H between radii $r_{k_{\text{inf}}}$ and $r_{k_{\text{sup}}}$. The eigenperiod perturbation is

$$d_nT_l = \int_0^b \tilde{R}\delta P_1 \frac{dr}{\Delta H_1} + \int_b^a \tilde{R}\delta P_2 \frac{dr}{\Delta H_2}. \tag{B2}$$

By expressing the continuity condition at $r = b$ we obtain

$$p_1 + x_1 p_2 + x_1^2 p_3 = p_4 + x_2 p_5 + x_2^2 p_6. \tag{B3}$$

If we now impose $x_1(b) = x_2(b) = 0$, which is equivalent to taking $r_{H_1} = R_{H_2} = b$ we obtain the very simple condition $p_1 = p_4$. Therefore, this kind of continuity condition is very easy to handle, by choosing the reference depth in each layer as the interface between the two layers. The inverse problem can then be reformulated as

$$\delta_nT_l = p_1 \int_0^a \tilde{R}\frac{dr}{\Delta H_1} + p_2 \int_0^b \tilde{R}x_1 \frac{dr}{\Delta H_1} + p_3 \int_0^b \tilde{R}x_1^2 \frac{dr}{\Delta H_1} + p_5 \int_b^a \tilde{R}x_2 \frac{dr}{\Delta H_2} + p_6 \int_b^a \tilde{R}x_2^2 \frac{dr}{\Delta H_2}. \tag{B4}$$